Lithos 202–203 (2014) 395–412

Contents lists available at ScienceDirect

Lithos

journal homepage: www.elsevier.com/locate/lithos

The Early Jurassic Bokan Mountain peralkaline granitic complex (southeastern Alaska): Geochemistry, petrogenesis and rare-metal mineralization

Jaroslav Dostal [a,*], Daniel J. Kontak [b], Susan M. Karl [c]

[a] Department of Geology, Saint Mary's University, Halifax, NS B3H 3C3, Canada
[b] Department of Earth Sciences, Laurentian University, Sudbury, ON P3E 2C6, Canada
[c] U.S. Geological Survey, Alaska Science Center, 4210 University Dr., Anchorage, AK 99508-4626, USA

ARTICLE INFO

Article history:
Received 12 December 2013
Accepted 7 June 2014
Available online 17 June 2014

Keywords:
Peralkaline granite
Rare earth elements
High field strength elements
Petrogenesis
Mineralization
Orthomagmatic hydrothermal fluids

ABSTRACT

The Early Jurassic (ca. 177 Ma) Bokan Mountain granitic complex, located on southern Prince of Wales Island, southernmost Alaska, cross-cuts Paleozoic igneous and metasedimentary rocks of the Alexander terrane of the North American Cordillera and was emplaced during a rifting event. The complex is a circular body (~3 km in diameter) of peralkaline granitic composition that has a core of arfvedsonite granite surrounded by aegirine granite. All the rock-forming minerals typically record a two-stage growth history and aegirine and arfvedsonite were the last major phases to crystallize from the magma. The Bokan granites and related dikes have SiO_2 from 72 to 78 wt.%, high iron ($FeO_{(tot)}$ ~3–4.5 wt.%) and alkali (8–10 wt.%) concentrations with high $FeO_{(tot)}/(FeO_{(tot)} + MgO)$ ratios (typically >0.95) and the molar $Al_2O_3/(Na_2O + K_2O)$ ratio <1. The granitic rocks are characterized by elevated contents of rare earth elements (REE), Th, U and high field strength elements (HFSE) and low contents of Ca, Sr, Ba and Eu, typical of peralkaline granites. The granites have high positive ε_{Nd} values which are indicative of a mantle signature. The parent magma is inferred to be derived from an earlier metasomatized lithospheric mantle by low degrees of partial melting and generated the Bokan granitic melt through extensive fractional crystallization. The Bokan complex hosts significant rare-metal (REE, Y, U, Th, Nb) mineralization that is related to the late-stage crystallization history of the complex which involved the overlap of emplacement of felsic dikes, including pegmatite bodies, and generation of orthomagmatic fluids. The abundances of REE, HFSE, U and Th as well as Pb and Nd isotopic values of the pluton and dikes were modified by orthomagmatic hydrothermal fluids highly enriched in the strongly incompatible trace elements, which also escaped along zones of structural weakness to generate rare-metal mineralization. The latter was deposited in two stages: the first relates to the latest stage of magma emplacement and is associated with felsic dikes that intruded along the faults and shear deformations, whereas the second stage involved ingress of hydrothermal fluids that both remobilized and enriched the initial magmatic mineralization. Mineralization is mostly composed of "new" minerals. Fluorine complexing played a role during the transportation of REE and HFSE in hydrothermal fluids and oxygen isotopes in the granites and quartz veins negate the significant incursion of an external fluid and support a dominantly orthomagmatic hydrothermal system. Many other REE–HFSE deposits hosted by peralkaline felsic rocks (nepheline syenites, peralkaline granites and peralkaline trachytes) were formed by a similar two stage process.

1. Introduction

Peralkaline granites are somewhat rare rock-types in the Earth's crust, but they attract a disproportionally large amount of attention in the geological literature because of their unusual geochemical characteristics and important economic potential (e.g., Bonin, 2007; Collins et al., 1982; Eby, 1990, 1992). These rocks frequently display a distinct enrichment in rare earth elements (REE), high field strength elements (HFSE) and radioactive elements (uranium and thorium) which, in some cases, are of economic significance (e.g., Cerny et al., 2005; Chakhmouradian and Zaitsev, 2012; Richardson and Birkett, 1996; Salvi and Williams-Jones, 2004). Controversy remains, however, regarding the origin of these silica-oversaturated alkaline magmas, as well as whether the contained mineralization (HFSE, REE, Th and U) is due to extensive fractional crystallization or is associated with the occurrence of late-stage magmatic–hydrothermal processes, which are common in these systems (e.g., Cerny et al., 2005; Marks et al., 2003; Salvi and Williams-Jones, 2004; Walters et al., 2013).

* Corresponding author. Tel.: +1 902 420 5747.
E-mail address: jdostal@smu.ca (J. Dostal).

http://dx.doi.org/10.1016/j.lithos.2014.06.005
0024-4937/

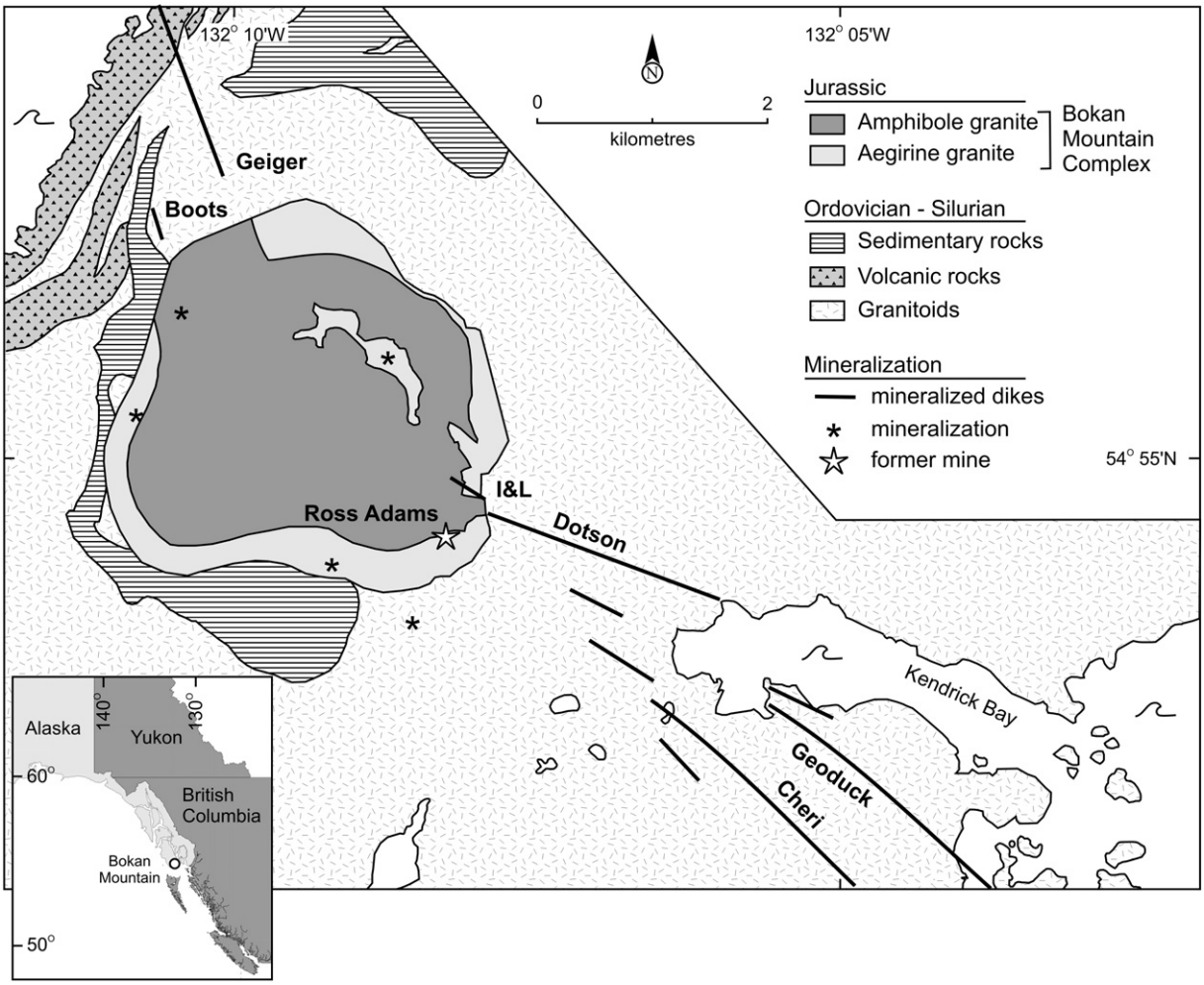

Fig. 1. Geological sketch map of the Bokan Mountain complex and surrounding area showing the location of the former mine and mineralization prospects referred to in the text (modified after Dostal et al., 2013; Gehrels, 1992; MacKevett, 1963; Thompson et al., 1982). The insert shows the location of the Bokan Mountain complex.

The Early Jurassic peralkaline granitic complex of Bokan Mountain (Fig. 1), located at the southern part of the Prince of Wales Island (southernmost southeast Alaska), hosts significant REE, HFSE, U and Th mineralization. The complex is well exposed and displays many structural and compositional features typical of anorogenic granitic complexes world-wide (e.g., the Younger granite ring complexes of Nigeria, Bowden and Turner, 1985 and parts of the Arab Shield associated with the opening of the Red Sea, Stoeser, 1986): it formed in a rift-related setting (Dostal et al., 2013), has a circular shape with associated dikes (Fig. 1), formed in a shallow-level setting, and the granites are peralkaline and characterized by high whole-rock Fe/Mg ratios and rare metal enrichment. In addition, the Bokan rocks also contain modal alkali amphibole and/or alkali pyroxene which reflect their peralkaline chemical signature.

The Bokan Mountain granitic complex hosts the former Ross–Adams mine, the only uranium producer to date from Alaska (Long et al., 2010). This mine, which was in operation intermittently between 1957 and 1971, produced about 77,000 t of high-grade uranium ore that averaged about 1 wt.% U_3O_8 and nearly 3 wt.% ThO_2 (Long et al., 2010). In addition to U and Th, economically significant levels of REE, Y, Nb and Zr mineralization have been documented in this granitic complex and petrogenetically related dikes (Dostal et al., 2011, 2013; Long et al., 2010; Robinson et al., 2011; Warner and Barker, 1989).

The purpose of this paper is to present data on the petrography, major- and trace element chemistry, and radiogenic and stable isotopes of the Jurassic Bokan granites. These data are then used to evaluate the origin of the parental magma of the Bokan Mountain complex, the processes that account for the geochemical evolution of the complex, including the origin of extreme trace element enrichment in both this and other similar types of granites, and to comment on the origin of the rare-metal mineralization.

2. Geological setting

The Bokan Mountain granitic complex (BMC), a crudely circular intrusion about 3 km in diameter, cross-cuts rocks of the Alexander terrane of the North American Cordillera. The BMC (Fig. 1) intrudes Ordovician–Early Silurian metasedimentary and metavolcanic rocks of the informally named Moira Sound unit (Slack et al., 2007) and Ordovician–Early Silurian granitoid rocks (Gehrels, 1992). The rocks of the Moira Sound unit unconformably overlie the Neoproterozoic to Lower Cambrian Wales Group which is composed of juvenile arc-related volcanic rocks, sedimentary sequences and granitoid intrusions (Ayuso et al., 2007; Samson et al., 1989). Stratigraphic rock units on Prince of Wales Island (PWI) are of Neoproterozoic and Paleozoic age. Mesozoic rocks in the southern part of PWI consist only of plutonic rocks, the oldest of which are the Early Jurassic Bokan Mountain and Dora Bay peralkaline granite complexes. The emplacement of the BMC was synchronous with other magmatic centres in the Alexander terrane, including the

Dora Bay pluton, located about 30 km north of the BMC, suggesting a regional but localized rifting event (Dostal et al., 2013). The Alexander terrane was accreted to the western margin of North America (Laurentia) subsequent to emplacement of the BMC, during the Late Mesozoic (Dostal et al., 2013). The emplacement of the BMC is constrained to 177 ± 1 Ma based on U–Pb zircon dating; its subsequent cooling history through ca. 450–500 °C occurred by 176 ± 1 Ma based on Ar–Ar dating of amphibole which was synchronous with mineralization associated with nearly vertical pegmatites, aplites and quartz–aegirine–fluorite veins and late-stage shear zones (Dostal et al., 2013). The contacts of the BMC with country rocks are sharp with generally steep dips that are inclined outward from the complex. This complex cuts the foliation in the andalusite-bearing hornfels and the granitoid country rocks; an extensive area of albitization extends outwards for up to 2 km from the contact. The albitization of the country rock granites is reflected by replacement of plagioclase and is accompanied locally by silicification. This alteration, which is most intense around the contacts with the pluton, was probably produced by infiltration of hydrothermal fluids related to the pluton.

There are two main types of rare-metal mineralization related to the Bokan complex. The first type includes felsic, aplitic and pegmatitic dikes and occurs within or adjacent to the BMC, whereas the second type is confined to a shear zone and encompasses the past producing Ross–Adams uranium deposit. In the central part of the BMC, the mineralization of the first type occurs within pegmatite dikes up to 10 m thick and 100 m long (Barker and Van Gosen, 2012). Along the periphery and adjacent to the BMC, this mineralization is also associated with felsic dikes, lenticular bodies and elongated pods, which range from <1 cm to about 3 m in width. The mineralized dikes commonly show bifurcating, anastomosing, feathering, and pinch out structures that tend to be localized along km-scale shear zones. Most of these dikes are associated with NW-trending shear zones and in rare cases may extend up to 5 km from the main pluton; in the latter cases the dikes become thinner with increasing distance from the main pluton. The mineralized dikes (vein-dikes of Warner and Barker, 1989) carry most of the REE, Y and HFSE mineralization and include the Dotson, I&L, Cheri, Geiger, Boots and Geoduck zones (Fig. 1). The second type of mineralization, which is inferred to be synchronous with the first type, is represented by the Ross–Adams U–Th deposit (Fig. 1). The deposit occurs within the BMC in a NW-trending shear zone that contains en echelon pods of ore. This pipe-shaped deposit is about 24 m thick and was mined along its strike for >300 m (Long et al., 2010; Thompson, 1988); the nature of the U–Th mineralization was discussed in some detail by Thompson (1988) and Cuney and Kyser (2008). The focus of this paper is on the processes associated with REE–HFSE mineralization.

3. Petrography

The granitic rocks of the BMC are generally leucocratic and typically contain about 2–10 vol.% mafic minerals, including sodic amphibole (i.e., arfvedsonite) and sodic clinopyroxene (i.e., aegirine; see Dostal et al. (2011) for mineral chemical data). The BMC (Fig. 1) is composed of two prominent zones: (1) a core which forms the main part of the complex and is comprised of arfvedsonite granite, and (2) an outer zone consisting of aegirine granite forming a nearly complete rim about 180 m thick. Locally, the aegirine granite grades into arfvedsonite granite; this transition occurs over about 15 m.

The granites include diverse rock types that range from saccharoidal aplites to prevalent medium- to coarse-grained granites and the dominant textures are primary porphyritic and late protoclastic (MacKevett, 1963). The porphyritic texture is characterized by phenocrysts of subhedral to euhedral quartz and K-feldspar ($Or_{>96}$) of 0.5 to 2 cm size that are enclosed in a fine- or medium-grained (typically 0.1–1 mm) quartzo-feldspathic groundmass with abundant albite. The protoclastic texture displays broken or granulated (cataclasized) phenocrysts of quartz and K-feldspar with offsets and bending of twinning and distinct undulose extinction of quartz. This texture is particularly well developed within broad, meter-scale shear zones that cross the pluton.

The granitic rocks are composed mainly of quartz (~35–45 vol.%), K-feldspar (microperthite and microcline) (35–50 vol.%) and plagioclase (5–15 vol.%); the latter occurs as both a separate phase (An_{20}) and as an intergrowth or replacement of K-feldspar. Representative photomicrographs of these mineral phases are shown in Fig. 2. Quartz appears to have formed during two stages, one magmatic and the other related to late-stage superimposed stress. The early quartz occurs as euhedral megacrysts, whereas the later occurs as grains within the matrix and as vein-like features. These thin quartz veinlets intersect both quartz and feldspars or occur as thin septae following cleavage in amphibole. There are two generations of K-feldspar: an early phenocrystic phase, now occurring as cross-hatched microcline that may be enclosed/embayed by microperthitic feldspar, and a matrix phase that commonly occurs as microcline. The coarser K-feldspar contains a variety of perthitic textures, including rare film and more common flame and bead types, and is both rimmed by albitic plagioclase (chess-board variety) and also variably replaced by albite throughout. The matrix K-feldspar lacks perthite texture, but is also variably replaced by albite. Plagioclase forms relatively fresh euhedral crystals, probably post-dating the first generation quartz and K-feldspar. In rare cases, the coarser plagioclase retains its primary magmatic composition (An_{20}), whereas all other plagioclase is albitic (<An_{10}) and, hence, is referred to simply as albite. Albite pervasively replaces K-feldspar, both as phenocrysts (particularly along the fractures) and in the groundmass. The groundmass is dominated by albite and quartz with lesser K-feldspar. The textural and compositional spectrum of plagioclase, now dominantly of albitic composition, reflects its formation from early magmatic crystallization to later fluid-mediated growth. The metasomatic nature of the feldspars is also indicated by the abundance of pitted textures present within these phases (Fig. 2f) and the local abundance of secondary fluid inclusions.

Although sodic amphibole ($Fe^{2+}/[Fe^{2+} + Mg] > 0.99$; arfvedsonite) and sodic pyroxene ($Jd_{13-19}Ae_{81-86}Di_{<1}$; $Fe/[Fe + Mg] > 0.99$; aegirine) are subordinate constituents of the granites, locally, they constitute up to about 30 vol.% of the rocks (i.e., some of the granites are mesocratic); representative photomicrographs are shown in Fig. 3. Generally both amphibole and pyroxene are spatially associated with one another, but in some samples only one or the other is present. Both of these phases may be poikilitic with inclusions of quartz, albite and microcline. Arfvedsonite, with characteristic pleochroism (lilac to blue), forms subhedral prismatic crystals typically 1–4 mm long, but rarely reaching >1 cm. The arfvedsonite crystals are interstitial, but fretted outlines indicate their continued growth into the matrix, possibly at a subsolidus stage (Fig. 3a,b,c), and they may rarely contain low-density fluid inclusions in their core (Fig. 3) which indicates that it is a late magmatic phase. The arfvedsonite may be replaced pseudomorphically by a fine-grained mixture of secondary minerals, most often quartz-hematite ± blue amphibole (Figs. 3e and 4), and in such cases it is common to find rare element mineralization in these domains (Fig. 4).

Subhedral sodic amphibole crystals typically record a two-stage growth history. Stage I is characterized by being inclusion-rich with melt, fluid and solid inclusions, whereas stage II represents an inclusion-free overgrowth (Fig. 3b). In places, stage I amphibole is overgrown by stage II aegirine. Likewise, inclusion-rich (fluid and melt inclusions) aegirine is commonly overgrown with clear inclusion-free aegirine. Notwithstanding the felsic composition of these rocks, the sodic pyroxenes and amphiboles commonly display a (sub)ophitic texture (i.e., they enclose or partly enclose euhedral albite crystals). Aegirine also occurs as intergranular needles,

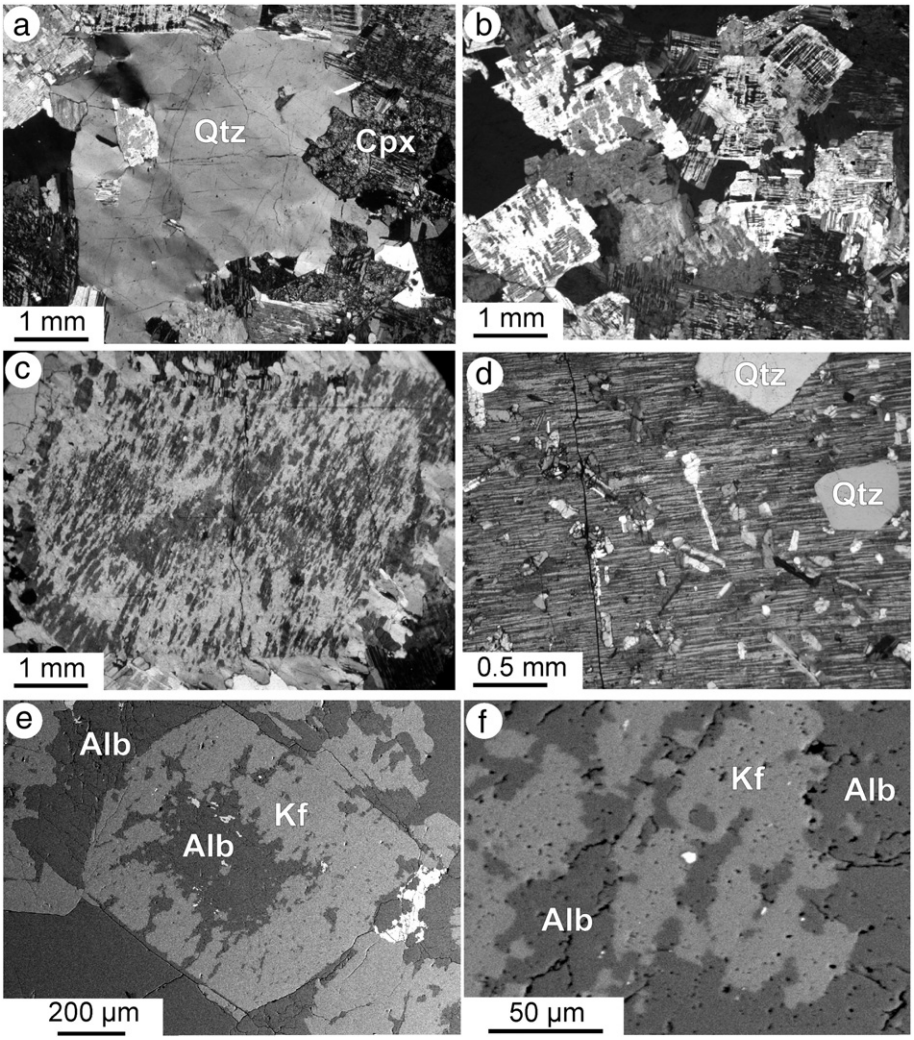

Fig. 2. Photomicrographs (all in cross nicols, Figures a to d) and scanning electron microscope (SEM) images (Figures e and f) of granitic rocks from the Bokan Mountain complex. showing the textures of the felsic phases. (a) Typical hypidiomorphic granular texture of the granite with coarse, mosaic-textured quartz in a quartz-two feldspar (plagioclase, microcline) matrix. Note the presence of aegirine in the right side of the image; (b) Typical metasomatic texture in the granites with extensive development of secondary albite after earlier K-feldspar, now microcline; (c) Sodic (albite) alteration of K-feldspar; (d) Part of a coarse (cm-size) grain of microcline perthite in a pegmatite with grains of euhedral albite laths and quartz. Note the well-developed film to flame type perthite lamellae in the microcline; (e) Euhedral K-feldspar being replaced by albite in the core and along radial fractures; (f) Extensively pitted K-feldspar and albite grains. Abbreviations: Qtz — quartz, Cpx — clinopyroxene, Alb — albite, Kf — K-feldspar.

spherulites and fracture-fills. Where both mafic minerals are present, it is not uncommon for the arfvedsonite to partly enclose and corrode the aegirine; however, in many cases pyroxene also post-dates amphibole. Another important observation is the occurrence of arfvedsonite with aegirine rims within meter-scale shear zones across the pluton; this texture also occurs near the pluton margin. In some samples, idiomorphic aegirine is enclosed by arfvedsonite, which itself is partly mantled by aegirine, which suggests alternating crystallization of these phases.

Accessory mineral phases, such as zircon, monazite, xenotime, titanite, fluorite and Fe–Ti oxide, are ubiquitous in the BMC granitic rocks. More than twenty REE-, HFSE- and U–Th-bearing minerals have been identified at the Bokan complex and its dikes (e.g., Philpotts et al., 1998; Staatz, 1978), and we have confirmed most of these in our study (Dostal et al., 2011). Importantly, these phases are present in altered granites in addition to ore-grade material. The dikes, particularly those of the I&L and Dotson zones, contain higher abundances of these minerals than the main pluton and many of these minerals occur in two or more generations. For example, zircon occurs not only as primary, colorless to pale yellow crystals but also as strings of grains along fractures or as crystals with texturally distinct cores. The post-magmatic zircon crystals are porous in appearances or form coating within the minor cavities and differ in composition from the primary zircon (Dostal et al., 2011).

In mineralized dikes, the REE, yttrium and HFSE mineralization has complex mineral assemblages which frequently consist of intergrowths, pseudomorphs, cavity and fracture fillings and mineral rims (see Dostal et al., 2011 for detailed description). The mineralization is contained in a variety of silicates, fluorocarbonates (bastnäsite, synchysite and parasite), oxides (columbite–tantalite, aeschynite, polycrase, pyrochlore, fergusonite) and phosphates (monazite, xenotime). The dominant REE silicates include iimoriite, zircon, kainosite, cerite, allanite and uranothorite (Table 1; Fig. 5). Uranium and Th in these dikes reside mainly in uranothorite, uraninite and coffinite (Table 1). The main ore minerals of the Ross–Adams deposit are uranothorite and uraninite with minor brannerite and coffinite and they are commonly enclosed in hematized and strongly altered and micro-fractured peralkaline granite with numerous ore-bearing veinlets that range from 0.1 to 1 mm thick and ovoids (0.2–2 mm across) (Thompson, 1988). The

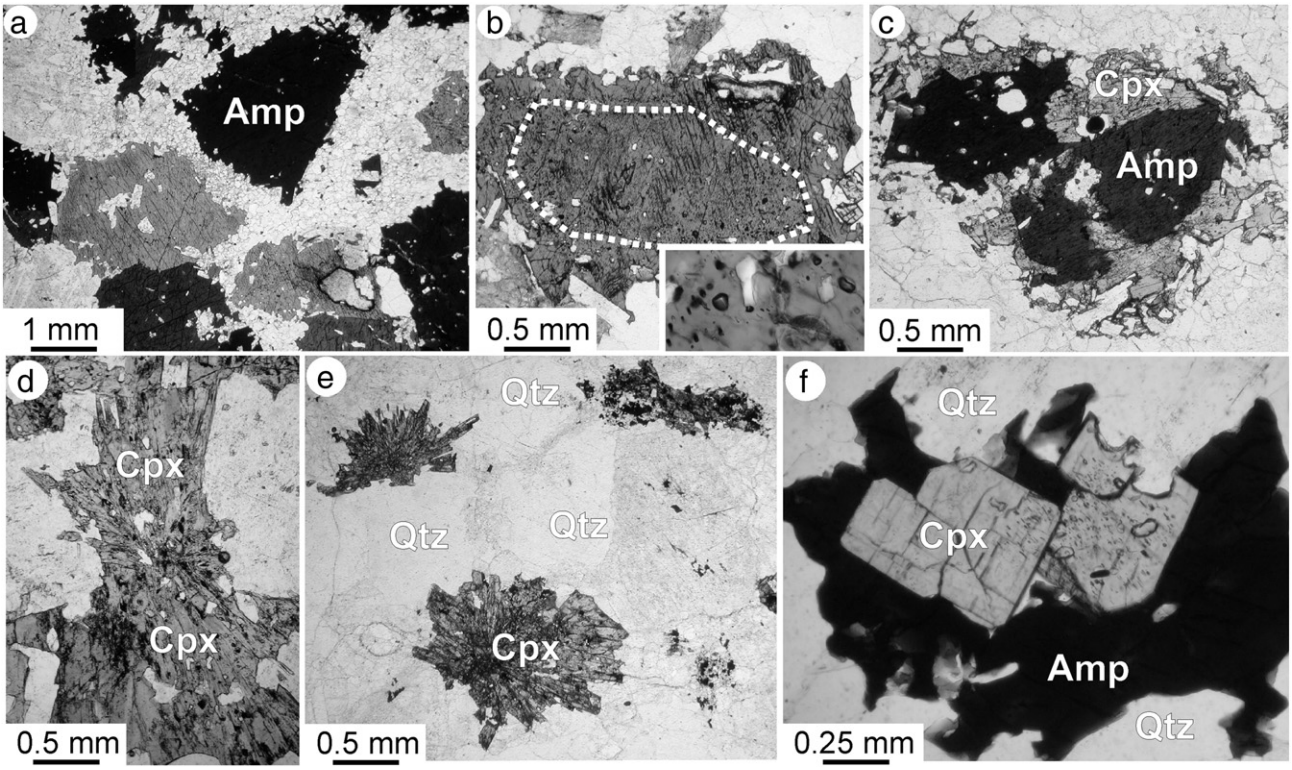

Fig. 3. Photomicrographs (all in plane polarized light) of granitic rocks from the Bokan intrusive complex showing the textures of the mafic phases. (a) Coarse subhedral amphibole grains set in a matrix of quartz and feldspar. Note the fritted edges to the amphibole grains that extend into the matrix; (b) Subhedral amphibole grain recording a two-stage growth history as indicated by the dashed white line. Stage I is characterized by an enrichment in inclusions, including possible melt, fluid and mineral (see inset for detail), whereas stage II is an inclusion-free overgrowth. Again, note the fritted outline of the grain along its top; (c) Subhedral arfvedsonite overgrown by aegirine with ragged terminations extending into the matrix. Note that the pyroxene partly replaces the amphibole; (d) Late-stage intergranular aegirine with a bowtie-like texture between coarser quartz and feldspar grains. Note the variable development of pleochroism and alteration along cleavage directions; (e) Radial-textured aegirine clots disseminated within a quartz–feldspar matrix and surrounding subhedral quartz (Qtz). Also note the intergrowth of amphibole–pyroxene with superimposed alteration (quartz-hematite) in the upper left of the image; (f) Euhedral aegirine overgrown by arfvedsonite. Note that the alignment (NW–SE) of secondary fluid inclusions in the pyroxene (right side) may be due to the overgrowth by the surrounding amphibole. Abbreviations: Qtz — quartz, Cpx — clinopyroxene, Amp — amphibole.

ore minerals are frequently associated with a minor amounts (<2 vol.%) of sulfides (pyrrhotite, pyrite, chalcopyrite, sphalerite, galena) and elevated concentrations of REE.

4. Major and trace element geochemistry

The granitic rocks of the Bokan complex (Appendix 2) have SiO_2 from 72 to 78 wt.% (Fig. 6a) which is accompanied by high iron ($FeO_{(total)}$ ~3–4.5 wt.%) and alkali ($Na_2O + K_2O$ ~ 8–10 wt.%) concentrations. Alumina varies from 10 to 13 wt.% and TiO_2 from 0.05 to 0.2 wt.%. The rocks are low in MgO (<0.04 wt.%) and CaO (<0.2 wt.%). The granites are peralkaline with both the aluminum saturation index (molar $Al_2O_3/(CaO + Na_2O + K_2O)$) and agpaitic index (molar $Al_2O_3/(Na_2O + K_2O)$) < 1 (Fig. 6b). The granites also have high $FeO_{(tot)}/(FeO_{(tot)} + MgO)$ ratios (typically > 0.95) and correspond to the ferroan granites of Frost et al. (2001). The samples compositionally resemble other peralkaline A-type granites (e.g., Bonin, 2007; Eby, 1990, 1992; Frost and Frost, 2011; Linnen and Cuney, 2004). The felsic dike rocks of the I&L and Dotson zones (Appendix 2) are compositionally similar to the main granite mass of the Bokan complex. Significantly, all the rocks of the BMC are geochemically distinct from the Paleozoic peraluminous and metaluminous granitoid country rocks (Fig. 6b).

The Bokan rocks are distinctly enriched in REE, Th, U and HFSE, but depleted in Ba, Sr and Eu (Fig. 7). The concentrations of Ba (<80 ppm) and Sr (<20 ppm) are very low (Appendix 2). The abundances of Rb (150–350 ppm) are high and are accompanied by low K/Rb ratios (100–250) relative to the continental upper-crustal average (~250; Taylor and McLennan, 1985). The noted depletion of Ba, Sr and Eu in peralkaline granitic rocks is usually attributed to the fractionation of feldspars, whereas Rb is highly incompatible and gradually enriched in late-stage melts (Abdel-Rahman, 2006; Cerny et al., 1985). The Bokan peralkaline granites have high Rb/Sr ratios (>5), similar to other anorogenic granites on the Rb/Sr vs K/Rb plot (Fig. 8).

The abundances of Zr (800–3000 ppm) and Nb (35–85 ppm) are high compared to typical orogenic granites (Linnen and Cuney, 2004; Winter, 2001) but within the range of peralkaline granites for Zr (800–14,000 ppm Zr, Linnen and Cuney, 2004) and lower for Nb (220–5750 ppm Nb, Linnen and Cuney, 2004). However, the average of the mineralized zones of the BMC is high — Zr ~ 1870 ppm and Nb ~ 443 ppm (Robinson et al., 2011). The enrichment in HFSE, which are mostly hosted in accessory phases, is a characteristic feature of peralkaline granites in general (e.g., Schmitt et al., 2002; Whalen et al., 1987). The Zr/Hf ratio typically varies from 37 to 50 and Nb/Ta ratios from 12 to 15, comparable to other anorogenic granitic complexes (e.g., Abdel-Rahman, 2006; Dostal and Chatterjee, 2000; Linnen and Cuney, 2004; Schmitt et al., 2002). In the BMC, as in some other peralkaline granitic complexes, the Nb/Ta ratio remains approximately constant, whereas the ratio decreases with increasing fractionation and Ta contents (Fig. 9) in peraluminous granitic rocks, such as those from the Devonian Davis Lake pluton of Nova Scotia (Dostal and Chatterjee, 1995). This difference in the Nb/Ta ratio during fractionation is probably related to the contrasting solubility of columbite–tantalite in

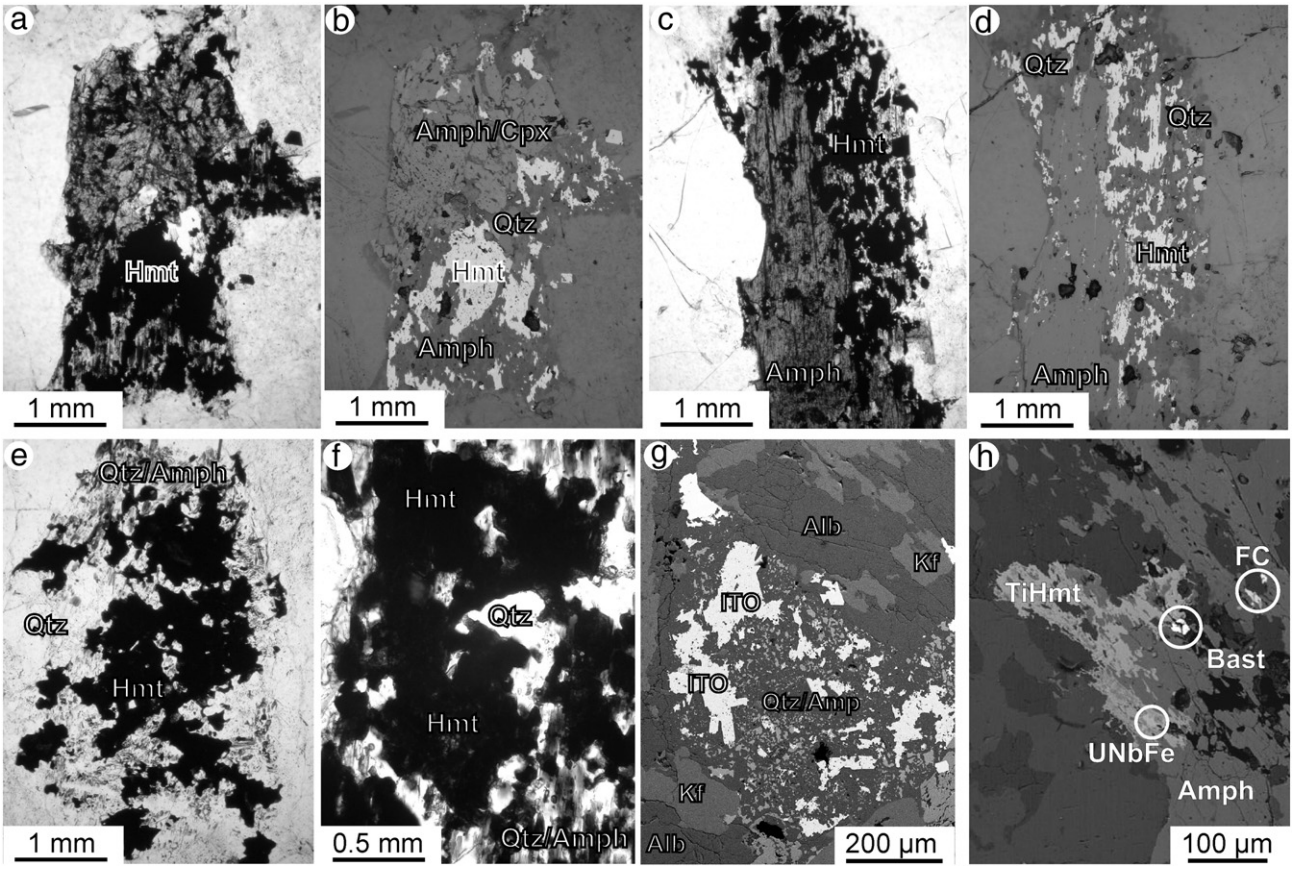

Fig. 4. Photomicrographs of altered and mineralized granitic rocks in plane polarized light (a, c, e, f), reflected light (b, d) and scanning electron microscopy (SEM; g, h). Note that images a–b and c–d are paired photos. (a, b) Subhedral outline of intergrown amphibole and clinopyroxene which have been replaced by quartz and hematite with a second generation blue amphibole also present in the bottom of the images. Note that it is mainly the amphibole area which is altered to hematite. (c, d) As in the previous images, but in this case the sample is inferred to have been entirely amphibole which is altered to an intergrowth of quartz and hematite. (e, f) Images of primary arfvedsonite completely pseudomorphed to an assemblage of quartz–hematite and second generation arfvedsonite. Image f is a close up the central part of image e. (g) SEM image of altered amphibole showing coarse Fe–Ti oxides with small residual grains of resorbed amphibole disseminated in quartz. (h) SEM image of altered amphibole with intergrowth titaniferous (6 wt.% Ti) hematite (TiHmt) and disseminated grains of a U–Nb–Pb hematite (UNbFe) phase, ferro-columbite and bastnäsite). Abbreviations: Qtz — quartz, Alb — albite, Kf — K-feldspar, Cpx — clinopyroxene, Amp — amphibole, Hmt — hematite, IOT — Fe–Ti oxides, Bast — bastnaesite., FC — ferro-columite.

peralkaline and peraluminous granites (Linnen and Keppler, 1997; Schmitt et al., 2002).

The Bokan granites also have high Ga contents (37–47 ppm) and high Ga/Al ratios (with $10^4 \times$ Ga/Al from 6 to 8), values typical of A-type granites (Whalen et al., 1987). Th and U abundances in the Bokan granites range from 7 to 58 ppm and between 2 and 27 ppm, respectively (Appendix 2), with average Th and U contents of about 24 and 12 ppm (Cuney and Kyser, 2008). These values are in a lower part of the ranges given by Linnen and Cuney (2004) for peralkaline granites (60–410 ppm Th and 8–155 ppm U). The average abundances of the Dotson zone are 91 ppm Th and 84 ppm U (Robinson et al., 2011). In the mineralized granites hosting the Ross–Adams deposit, the abundances are significantly higher ranging from 1180 to 27,000 ppm Th and from 80 to 17,400 ppm U (Cuney and Kyser, 2008). The fluorine content is high and variable (320–10,200 ppm; Cuney and Kyser, 2008) and is reflected in the widespread occurrence of fluorite, a common late-stage phase.

The REE abundances for the Bokan granites, particularly the heavy REE (HREE), are high and the $(La/Yb)_n$ ratios are variable (~0.7 to 8). The REE and Y vary by order of magnitude. The contents of Yb reach up to 55 ppm, Dy up to 60 ppm and Y up to 300 ppm. The shapes of the chondrite-normalized REE patterns (Fig. 7) range from those showing a small LREE enrichment [$(La/Sm)_n$ ~1–2] and nearly flat or gently sloping HREE [$(Gd/Yb)_n$ ~1–2], which are most common, to V-shaped patterns with distinct enrichments in LREE [$(La/Sm)_n$ ~4–5] and HREE [$(Gd/Yb)_n$ ~0.2] relative to middle REE (MREE) abundances. The samples with a positive MREE-to-HREE slope typically contain zircon and/or fergusonite, consistent with their preference for the HREE. The chondrite-normalized patterns of all the Bokan granites display a distinct negative Eu anomaly (Eu/Eu*), typically ~0.3, which implies extensive feldspar fractionation. In addition, the size of the Eu anomaly is similar in all samples which suggest that all samples have undergone a similar degree of feldspar fractionation.

On the primitive mantle normalized plots (Fig. 7), the Bokan peralkaline granites exhibit moderate enrichment in most of the HFSE and REE (including Y), as well as Th and Rb, but marked depletion in Sr, Eu, Ba and Ti. These mantle-normalized patterns for the BMC are comparable to patterns typical of peralkaline granites (Fig. 7). The granitic (including aplitic) rocks from the I&L and Dotson zones have many geochemical characteristics similar to samples from the main mass of the Bokan complex, but the average trace element concentrations of samples from the mineralized sections of these two zones differ (Fig. 10). The average compositions of the mineralized parts of the I&L zone are distinctly enriched in HREE with $(La/Yb)_n$ ~0.7, $(La/Sm)_n$ ~2 and $(Gd/Yb)_n$ ~ 0.4, whereas the average for the Dotson zone yields $(La/Yb)_n$ ~ 3, $(La/Sm)_n$ ~1.4 and $(Gd/Yb)_n$ ~1.7 (Robinson et al., 2011). Both averages have negative Eu anomalies which are of similar magnitude. In the Dotson zone, the La/Yb ratio of the mineralization decreases with distance from the complex (Robinson et al., 2011). The average REE abundances and pattern of the mineralized sections of the BMC

Table 1
Microprobe analyses (wt.%) of ore and accessory minerals.

Sample	Coffinite	Uranothorite	Bastnäsite	Synchysite	Iimoriite	Zircon	Zircon[2]
(wt%)							
SiO_2	19.7	17.5	0.06		17.1	28.0	33.4
TiO_2							0.33
Al_2O_3	1.06	0.43	0.02				0.08
FeO	0.62	0.92	0.20		0.92	0.21	0.26
CaO	0.50	1.61	2.84	16.2	0.09		0.11
ZrO_2	0.01	0.02	0.09		0.01	57.3	61.4
HfO_2	0.27	0.10	0.06		0.51	1.65	
Nb_2O_5	0.03	0.02	0.01			0.06	
PbO	0.10	0.15			0.40	0.08	
ThO_2	0.06	39.5	0.83	0.14	0.04	1.51	0.27
UO_2	64.9	30.3	0.07	0.03	0.06	1.57	0.38
Y_2O_3	9.50	1.16	2.06	16.9	45.4	3.05	2.40
La_2O_3	0.02	0.04	13.7	9.51	0.04	0.02	
Ce_2O_3	0.12	0.12	31.4	15.5	0.08	0.04	0.32
Pr_2O_3	0.03	0.05	4.56		0.06	0.03	
Nd_2O_3	0.07	0.04	12.5	5.61	0.09	0.03	
Sm_2O_3	0.05	0.09	2.00	1.11	0.21		
Eu_2O_3			0.65		0.08	0.01	
Gd_2O_3	0.40	0.08	3.96	2.46	1.82	0.03	
Tb_2O_3					0.62	0.05	
Dy_2O_3	1.15	0.29	0.62	2.49	6.64	0.79	
Ho_2O_3	0.23	0.18	0.11		1.64	0.46	
Er_2O_3	1.02	0.10	0.12	0.67	5.71	1.20	
Tm_2O_3	0.07	0.03	0.23		0.73	0.26	
Yb_2O_3	0.65	0.08		0.20	5.28	2.81	
F	0.71	0.39	5.13	3.19	0.12	0.15	
n	3	67	16	3	32	6	

The data (except zircon[2]) are averages of microprobe analyses of minerals separated during a processing of bulk sample of mineralized felsic dike from the I&L zone for metallurgical investigation (microprobe analyses done at the Department of Earth and Planetary Sciences, McGill University, Montreal, Quebec for Ucore Rare Metals); zircon[2] — Bokan peralkaline granite (sample G244; microprobe analysis done at the Department of Earth Sciences, Dalhousie University, Halifax); n — number of analyzed grains.

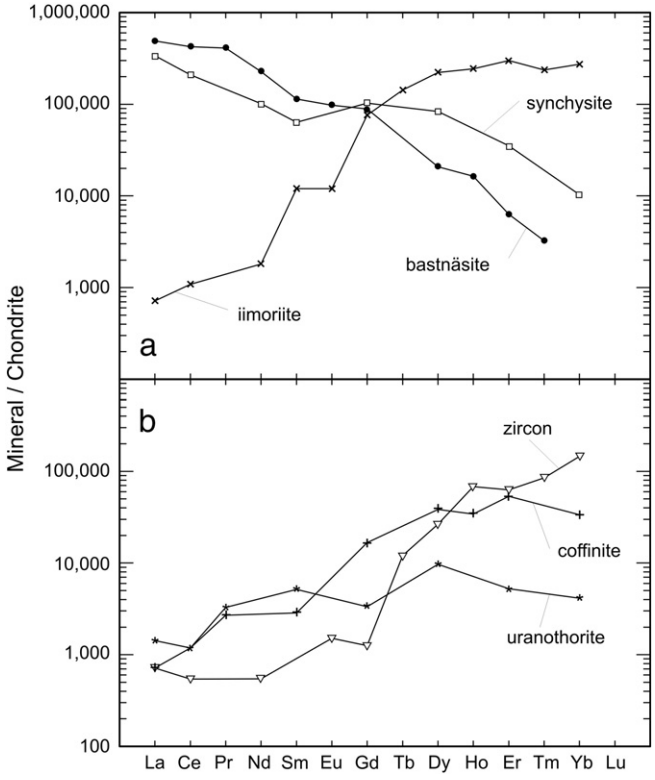

Fig. 5. Chondrite-normalized REE abundances of (a) bastnäsite, synchysite and iimoriite and (b) uranothorite, coffinite and zircon from the felsic dikes of the I&L zone. Normalizing values are C1 chondrite from Sun and McDonough (1989). Plotted data are averages of microprobe analyses of minerals (Table 1) separated during a processing of bulk samples for metallurgical investigations (archives of Ucore Rare Metals; microprobe analyses done at McGill University, Montreal, Quebec).

are comparable to those of some other REE deposits associated with peralkaline felsic rocks (Fig. 10).

5. Isotope geochemistry

5.1. Neodymium isotopes

Nd isotopic ratios for the rocks of the Bokan complex and related dikes are given in Table 2; they are all age-corrected to the time of formation of the BMC at 177 Ma. These data are in agreement with the values reported by Samson et al. (1989) and Philpotts et al. (1998) although the latter reported the ε_{Nd} values as high as +10 and +12. The similarities of the ε_{Nd} values of the Bokan complex and the Dotson and I&L dikes suggest that these rocks were derived from the same source. The high positive ε_{Nd} values (+2.7 to +6.6) for the granitic rocks of the Bokan complex and the dikes indicate that the rocks were derived from a reservoir with a history of LREE depletion, such as depleted upper mantle, and were not affected by contamination of ancient continental crust. However, the enrichment of LREE suggests that the inferred mantle source was metasomatically enriched at more recent times; LREE/HREE fractionation during partial melting and subsequent fractional crystallization, however, also need to be considered if inferences are to be made about the mantle source. Furthermore, the large variations of ε_{Nd} values (from +2.7 to +12) for the relatively homogeneous complex is evidence that during the late-stage evolution of the complex, F-rich fluids remobilized REE which resulted in a modification of the age-corrected Nd isotopic values.

5.2. Lead isotopes

Eleven whole rock samples of granitic and dike rock material from the BMC were analyzed for their Pb isotopic composition and U, Pb and Th contents. The results are reported in Table 3, where the Pb

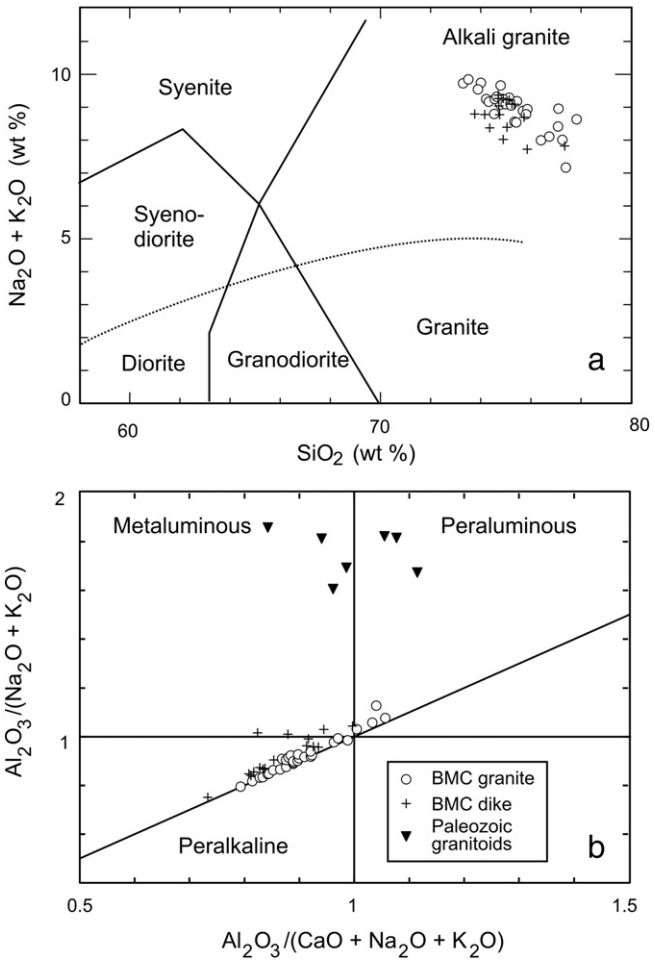

Fig. 6. (a) Binary plot of $Na_2O + K_2O$ (wt.%) versus SiO_2 (wt.%) for rocks of BMC; fields after Cox et al. (1979). The dotted line subdivides alkaline from subalkaline rocks. (b) Binary plot of molar $Al_2O_3/(Na_2O + K_2O)$ versus $Al_2O_3/(CaO + Na_2O + K_2O)$ that discriminates metaluminous, peraluminous and peralkaline compositions of granitic rocks. The analyses of the granitic rocks of the Bokan Mountain complex and related dikes are given in Appendix 2 while those of the Paleozoic country rock granitoids are from MacKevett (1963), Philpotts et al. (1998) and Dostal et al. (2011).

isotopic ratios are also age-corrected to 177 Ma using Parent/Daughter ratios calculated from ICP-MS measured U, Th and Pb concentrations. A galena sample from a pegmatitic dike of the I&L zone was also analyzed in this study. The Pb isotopic data are summarized on conventional $^{207}Pb/^{204}Pb$ versus $^{206}Pb/^{204}Pb$ and $^{208}Pb/^{204}Pb$ versus $^{206}Pb/^{204}Pb$ diagrams in Fig. 11, where the data are compared to the various lead evolution curves of Doe and Zartman (1979). Of note in these diagrams is the large range in $^{206}Pb/^{204}Pb$ values. Compared to the lead isotope evolution curves, the data fall below the orogene model growth curve in terms of the $^{207}Pb/^{204}Pb$ versus $^{206}Pb/^{204}Pb$ values. Furthermore, the distribution of the Pb isotopic data in $^{207}Pb/^{204}Pb$ versus $^{206}Pb/^{204}Pb$ space defines a slope (0.07356) which equates to a $^{207}Pb/^{206}Pb$ age of 1034 Ma. Although this regression has no significance in terms of absolute age, it does reflect the possible mixing of reservoirs. Importantly, the galena sample plots at the radiogenic end of the array.

A large range in initial (age-corrected) Pb isotopes cannot be readily explained by crustal contamination as it would require significantly variable contributions from contaminants which may be hard to reconcile with such an evolved and homogeneous magma. However, the spread of the age-corrected Pb isotopic values is more easily explained if the rocks were instead modified due to interaction with late-stage fluids which have changed the U/Pb and Th/Pb ratios. The age correction of measured Pb isotopes assumes that measured Parent/Daughter (U/Pb, Th/Pb) ratios are the result of in situ growth of radiogenic Pb from their parent with a proportional change in the original magmatic U/Pb and Th/Pb ratios. However, these ratios have likely been affected by the ingress of late-stage fluids which changed the concentrations of Th and U. Thus, for example, late- to post-magmatic modification of (U, Th)/Pb ratios yields the widely disparate age-corrected $^{206}Pb/^{204}Pb$ ratios. It is also possible that the alteration, in part, occurred during the subsolidus evolution of the complex which involved fluid: rock interaction, as recorded in the petrographic features of the rocks. The lead isotopic system was, therefore, significantly disturbed by hydrothermal fluids/metasomatic processes.

The galena sample is considered to be the best approximate of the isotopic composition of lead in the melt and fluids at the time of crystallization of the BMC and formation of related orthomagmatic mineralization. The array defined, which provides a geologically meaningless age of 1034 Ma, is an artifact of mixing of lead cognate to the BMC and an external source of lead which we infer to be from the surrounding, older basement rocks. The latter lead is evidence, therefore, of the ingress of a fluid which interacted with this reservoir.

5.3. Oxygen isotopes

Seven samples of quartz from granitic material were analyzed for their $\delta^{18}O_{V\text{-}SMOW}$ values. The reason for analyzing quartz is that analysis of whole rock samples of material often records post-magmatic fluid: rock exchange and re-equilibration of the sample where feldspars account for a large proportion of the rock (e.g., Cathles, 1993). The quartz came from two samples of amphibole granite and five samples of vein and pegmatite and the results of the analyses are summarized in Table 4. The $\delta^{18}O_{V\text{-}SMOW}$ values for quartz from the two granitic samples are essentially identical with $\delta^{18}O_{V\text{-}SMOW}$ values of +9.0 and +8.9‰, whereas values of quartz from the second group range from +8.9 to +11.3‰ and average +9.7‰, but we note that one sample falls outside the narrower range of +8.9 to 9.7‰ which gives an average of +9.3‰.

In terms of the granitic samples, it is important to note that $\delta^{18}O_{V\text{-}SMOW}$ values of quartz do not vary much as a result of magmatic crystallization (Taylor and Sheppard, 1986), thus it can be inferred that the data for the two quartz samples are a good approximation of $\delta^{18}O_{quartz}$ for the Bokan granites and can be used to estimate the original composition of the melt. Based on a compilation of whole rock and quartz $\delta^{18}O$ values for a variety of granites from various settings, Kontak and Kyser (2009) estimated Δ quartz-whole rock = +1.2‰, which is consistent with the expected small crystal–melt partitioning of ^{18}O at a high temperature in magmas (Bottinga and Javoy, 1973; Taylor and Sheppard, 1986). For the average Bokan quartz, this suggests the melt had a $\delta^{18}O$ value of +7.8‰ which falls just above the range of +5 to +7‰ for mantle-derived melts (Kyser, 1986) and is, instead, more typical of I-type granites (Taylor, 1986).

The quartz data for the pegmatite and vein samples are similar to the quartz values from the granites, hence, it can be inferred that the melt compositions are also the same. The quartz data for the pegmatite and vein samples can also be used to evaluate the isotopic composition of the fluid phase, with which the quartz would be in equilibrium, thereby indirectly assessing its source. The narrow range of $\delta^{18}O$ data for the pegmatite-vein quartz samples provide an average value of +9.3‰ which indicates $\delta^{18}O_{H2O}$ values of +7 and +5.2‰ for exchange at 500° and 400 ºC, respectively (Matsuhisa et al., 1979), and fall in the range for normal magmatic waters (Sheppard, 1986). As for the single quartz sample with a value of +11.3‰, this sample may represent crystallization at a lower temperature than the other samples. For example, if the latter formed at 500 ºC then a 2‰ difference would require the former to have formed at 400 ºC. Thus, these oxygen isotopic data for pegmatite and vein samples are consistent with the generation of a

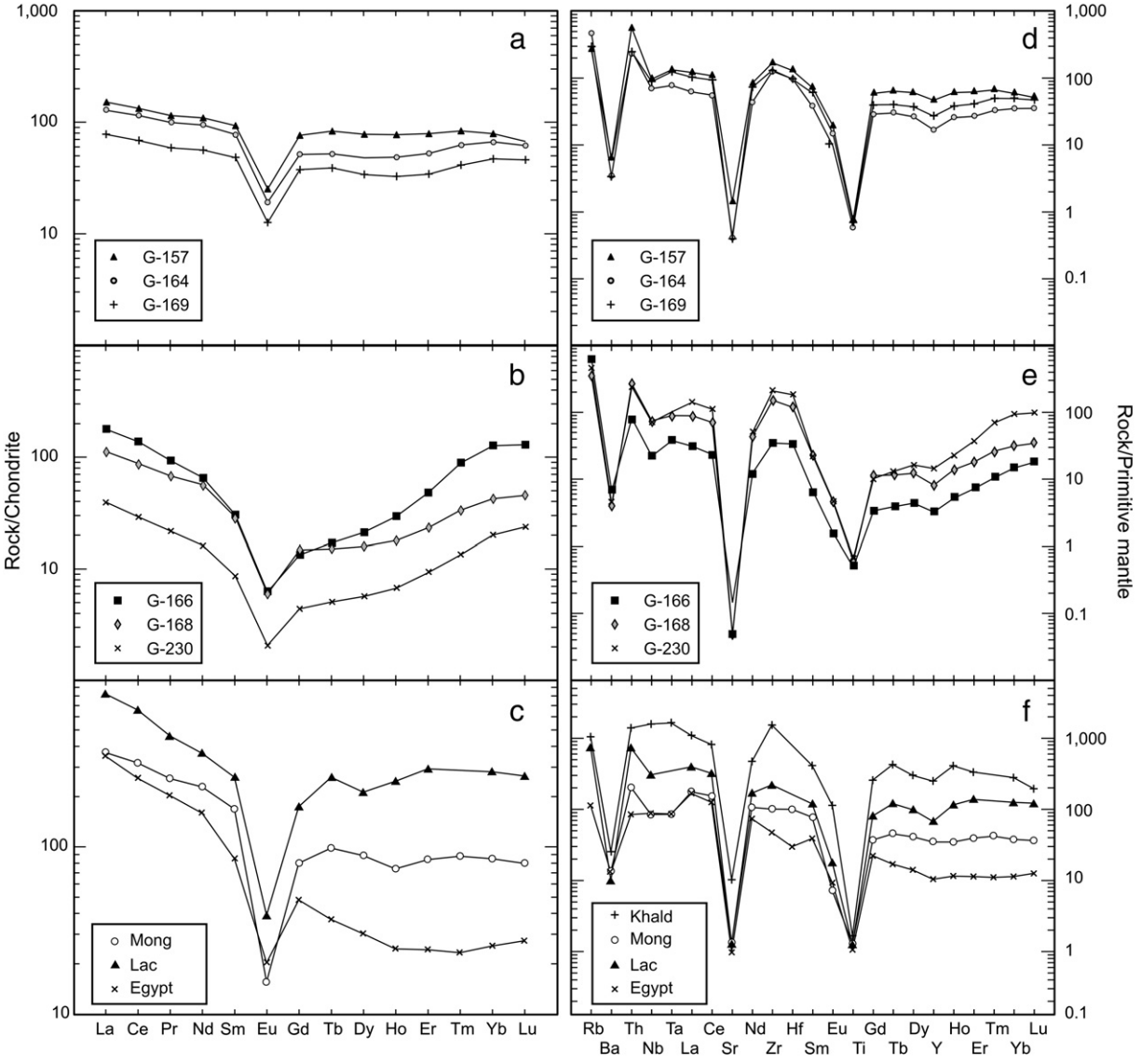

Fig. 7. a–c. Chondrite-normalized REE abundances in peralkaline granitic rocks. (a) Bokan granites with relatively flat to slightly LREE enriched patterns; (b) Bokan granites with LREE enrichment and a positive MREE/HREE slope; (c) Peralkaline granites: Egypt — average of peralkaline granites of eastern Egypt (Abdel-Rahman, 2006), Mong — average of the main phase granite of the Khan Bogd complex, southern Mongolia (Kynicky et al., 2011), Lac — peralkaline granite of the Lac Brisson, Labrador, Canada (Linnen and Cuney, 2004; Pillet et al., 1992). Normalizing values are C1 chondrite from Sun and McDonough (1989). d–f. Primitive mantle-normalized incompatible trace element abundances of the peralkaline granitic rocks. (d) Bokan granites with relatively flat to slightly LREE enriched patterns; (e) Bokan granites with LREE enrichment and a positive MREE/HREE slope; (f) Typical peralkaline granites: Egypt — average of peralkaline granites of eastern Egypt (Abdel-Rahman, 2006), Mong — average of the main phase granite of the Khan Bogd complex, southern Mongolia (Kynicky et al., 2011), Lac — peralkaline granite of the Lac Brisson, Labrador, Canada (Linnen and Cuney, 2004; Pillet et al., 1992); Khald — average of mineralized granite of the Khaldzan–Buregtey complex, western Mongolia (Kovalenko et al., 1995). Normalizing values are after Sun and McDonough (1989).

magmatic fluid in the BMC from a closed system and the current data set does not necessitate the incursion of external fluid during the late magmatic-early hydrothermal stage of evolution of the Bokan complex. A singular model involving cooling of an orthomagmatic fluid is therefore suggested. This is also in agreement with the oxygen and carbon isotopic data for carbonates from the Ross–Adams deposit reported by Thompson (1988), which indicate a magmatic origin.

6. Discussion

6.1. Petrogenesis of the peralkaline granites

The Bokan granites display features typical of peralkaline granites. These traits include: (1) the presence of alkali amphibole and alkali pyroxene in the mode, (2) molar $Al_2O_3/(Na_2O + K_2O) < 1$, (3) the presence of acmite in the CIPW norms (indicating an excess of $Na_2O + K_2O$ over Al_2O_3 (mole %)) and (4) trace element characteristics of peralkaline granites (high REE, HFSE, U and Th but low Ba, Sr and Eu and high Rb/Sr and 10^4Ga/Al relative to typical continental crust). The Bokan complex was emplaced during a regional but localized rifting event (Dostal et al., 2013).

6.1.1. Magma evolution

The compositional characteristics of the peralkaline granitic rocks of the Bokan complex, which include high Fe/Mg ratios, high contents of SiO_2, HFSE, REE, Th and U, as well as low contents of Sr, Ba and Eu, are consistent with a model of fractional crystallization of a peralkaline felsic magma leading to a strongly evolved

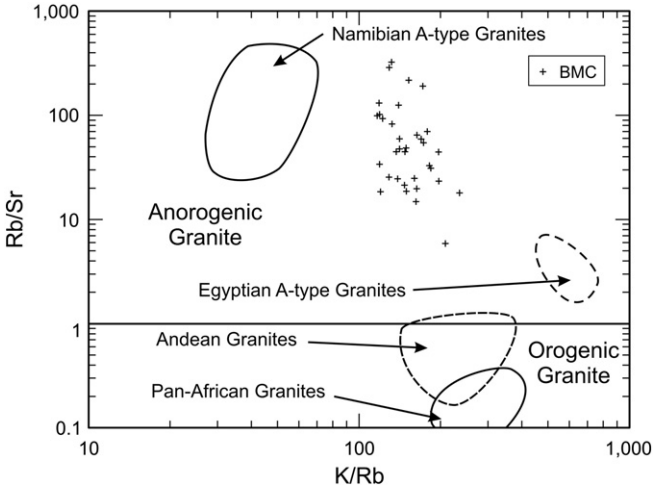

Fig. 8. Binary plot of ratios of Rb/Sr versus K/Rb showing that the fresh Bokan peralkaline granites (+ symbols; altered samples were not plotted) have Rb/Sr ratios > 1. The boundary (at Rb/Sr = 1) that separates the fields of orogenic and anorogenic granites as well as the fields for the orogenic, Pan-African and Andean granites and for the anorogenic granites of eastern Egypt and Namibia are after Abdel-Rahman (2006).

melt composition, in part due to the role of volatiles, which depress the solidus in the rock systems (e.g., Markl et al., 2001). Alkalis and fluorine also increase the solubility of HFSE, REE, Th and U in volatile-bearing peralkaline felsic magmas (Linnen and Keppler, 1997, 2002) and thereby contribute to the suppression of crystallization of HFSE- and REE-bearing accessory minerals until the latest stages of fractionation (Keppler, 1993; Linnen, 1998). The highly incompatible trace elements, in particular REE, U, Th, HFSE and Rb, are progressively enriched in the residual alkaline/peralkaline magmas during fractional crystallization leading to the high concentrations of these elements in evolved rocks such as those of the BMC.

Negative anomalies of Ba, Sr and Eu on the primitive mantle-normalized spidergram plots for the Bokan rocks (Fig. 7) reflect the fractionation of feldspars, whereas the depletion of Ti probably

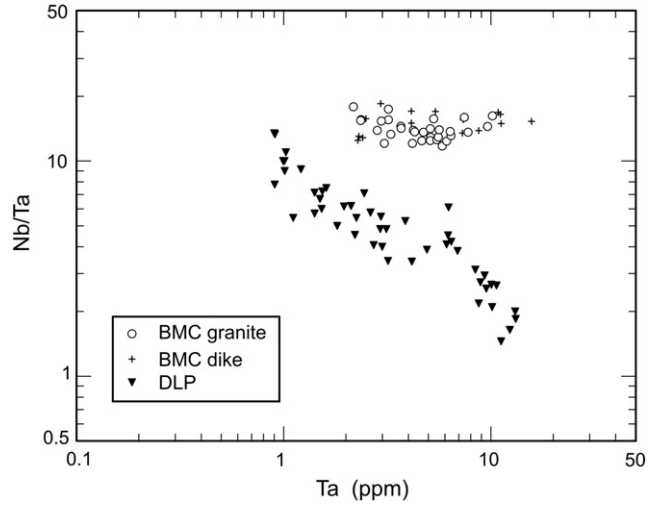

Fig. 9. Binary plot of the Nb/Ta ratio versus Ta (ppm) for the peralkaline granitic rocks of the Bokan Mountain complex (circles) and related dikes (crosses) and the peraluminous granitic rocks the Devonian Davis Lake pluton (solid triangles) of Nova Scotia (Dostal and Chatterjee, 1995, 2000).

reflects the fractionation of Fe–Ti oxides or titanite. Such spider diagrams suggest that these granites solidified from highly fractionated melts that underwent extensive low-pressure feldspar-dominated crystal fractionation. The distinct differences in the REE patterns and abundances among the rocks of similar major element compositions (Fig. 7, Appendix 2) are consistent with an important role of accessory minerals and fluids during the evolution of these rocks.

As the magma was poor in Mg and rich in Fe, the mafic minerals (aegirine and arfvedsonite) were very close to the Fe-end members and as such they were the last rock-forming minerals to crystallize from the magma. These minerals typically enclose accessory HFSE- and REE-bearing minerals (e.g., zircon and fergusonite). Initially, the magma was oxidized, as indicated by near end member aegirine. The late stages of crystallization were more reducing (but accompanied by higher water pressure) leading to the crystallization of arfvedsonite (with high proportion of Fe^{2+}) in lieu of aegirine but the conditions were variable as indicated by aegirine also locally replacing arfvedsonite. However, late stage hydrothermal replacement of mafic minerals by the association of hematite and quartz and extensive hematitization associated with mineralization indicate a subsequent post-magmatic/hydrothermal return to oxidizing conditions.

6.1.2. Source rock composition

Peralkaline/alkaline magmas are conventionally considered to be derived by low degrees of partial melting of a mantle source (e.g., Bonin, 2007; Pilet et al., 2008; Platt, 1996). Such mantle sources had to have high contents of incompatible trace elements relative to primitive mantle source and corresponded probably to metasomatically enriched lithospheric mantle (e.g., Pilet et al., 2008). However, there is still a controversy regarding the origin of peralkaline silica-oversaturated felsic rocks such as those of the Bokan complex. Several processes which have been proposed for the origin of the peralkaline granitic magmas and can be considered for the BMC, are: (1) crustal contamination of silica-undersaturated alkaline magmas (e.g., Goodenough et al., 2000; Halama et al., 2004; Marks and Markl, 2001); (2) melting of lower crust (including an underplated alkali basaltic source), possibly metasomatized by mantle-derived fluids (e.g., Bonin, 2007; Lentz, 1996; Martin and De Vito, 2005) and (3) melting of metasomatically enriched lithospheric mantle (e.g., Pilet et al., 2008; Upton et al., 2003).

Crustal contamination of a nepheline syenitic magma was invoked to explain the origin of quartz syenites of the Ilimaussaq complex of Greenland (Marks and Markl, 2001). Although it is possible that the parent magmas of the BMC experienced a limited degree of crustal contamination during the ascent to and/or residence in crustal magma chambers, it does not appear that the trace element and isotopic characteristics of the BMC peralkaline granites are due to crustal contamination. The absence of distinct negative Nb anomalies on the mantle normalized plots (Fig. 7), the consistently positive ε_{Nd} values and the lack of a correlation of ε_{Nd} values with contamination-sensitive indexes (e.g., SiO_2, $(La/Sm)_n$ and Eu/Eu^*), as well as oxygen isotopes, argue against extensive crustal contamination or assimilation-fractional crystallization processes. Likewise, a distinct enrichment of incompatible trace elements (ITE), as well as a peralkaline composition of the granites, is not readily consistent with assimilation by common crustal rocks/melts which are typically peraluminous and have significantly lower contents of ITE.

The other two models (melting of lower crust or lithospheric mantle) are plausible. However, quantitative geochemical modeling of these processes is hampered by the fact that some trace elements are prone to mobilization (Rb, Ba, K), whereas others (REE, Y, Th, U and HFSE) in addition to the Pb and Nd isotopes, were probably modified by hydrothermal fluids. Since the BMC granites are compositionally similar to some recent felsic volcanic rocks such as pantellerites

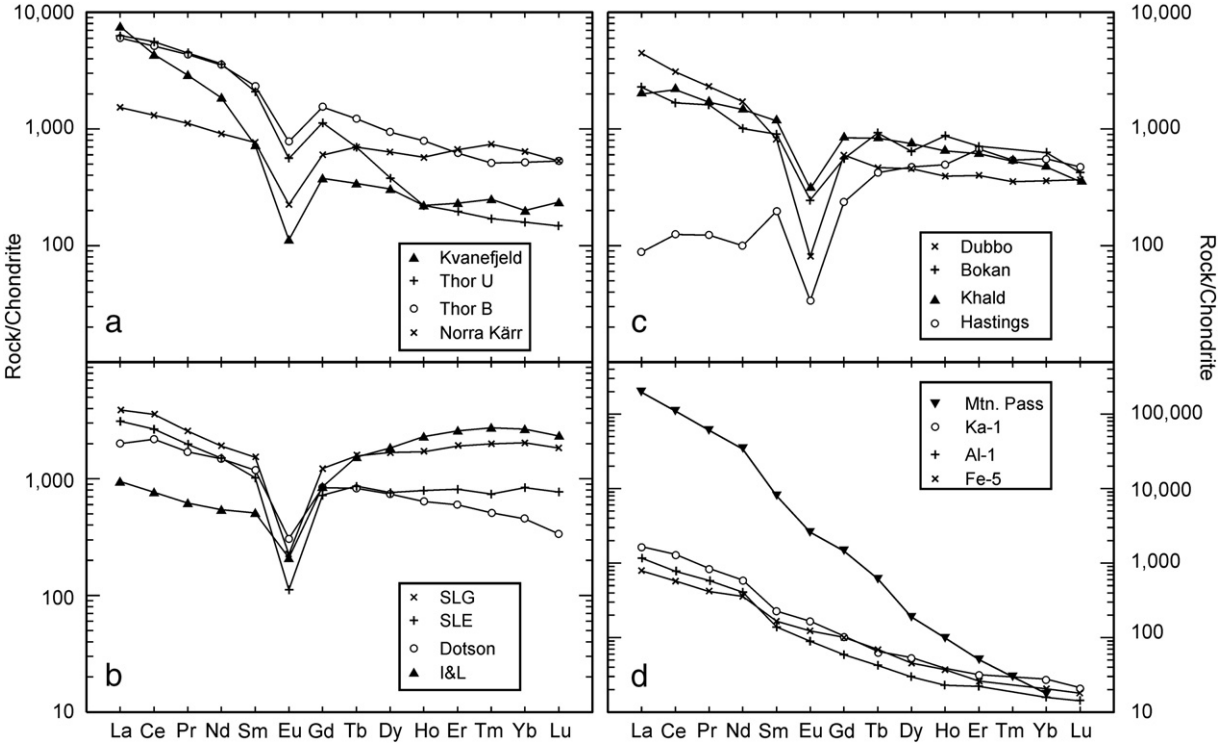

Fig. 10. Chondrite-normalized REE patterns for the averages of mineralizations hosted by peralkaline felsic rocks (a) deposits hosted by nepheline syenites (Kvanefjeld, Greenland; Norra Kärr, Sweden; Thor Lake/Nechalacho, Canada: Thor B — basal deposit; Thor U — upper deposit; (b) deposits hosted by peralkaline granites (Strange Lake, Canada: SLG — granite deposit, SLE — enriched deposit; Bokan, Alaska, USA: Dotson — Dotson zone; I&L — I&L zone — Robinson et al., 2011); (c) deposits hosted by peralkaline trachytes (Dubbo — Dubbo Zirconia, Australia and Hastings — Hastings/Brockman, Australia) and peralkaline granites (Bokan and Khald — average of mineralized granite of the Khaldzan – Buregtey, western Mongolia (Kovalenko et al., 1995)). The data with the exception of Khald, Dotson and I&L zones are from Hatch (2014); (d) mineralized carbonatites (Mtn. Pass — average ore of Mountain Pass deposit, California, Castor, 2008) as well as non-mineralized carbonatites (Hornig-Kjarsgaard, 1998): Ka-1 — carbonatite from Kaiserstuhl, Germany, Al-1 — carbonatite from Alnö, Sweden and Fe-5 — carbonatite from Fen, Norway). Normalizing values are after Sun and McDonough (1989).

(e.g., Civetta et al., 1998; Ronga et al., 2010), it can be suggested, by analogy, that like many pantellerites the Bokan granites plausibly represent the products of extensive fractionation of alkaline basaltic magma generated from small degrees of partial melting of a metasomatically enriched lithospheric mantle (e.g., Mungall and Martin, 1996; Upton et al., 2003). Such a mantle source of the parent melt of the Bokan complex had a prior history of metasomatic enrichment of incompatible trace elements, including the light REE, as also suggested by positive ε_{Nd} values.

6.2. Mineralization

6.2.1. Origin of REE and HFSE mineralization

The genesis of the REE and HFSE mineralization associated with the peralkaline felsic rocks is not well understood and debate remains as to whether the mineralization is magmatic, hydrothermal or a combination of the two (e.g., Cerny et al., 2005; Linnen and Cuney, 2004; Richardson and Birkett, 1996; Salvi and Williams-Jones, 1990, 1996, 2004). The magmatic model assumes that the enrichment is mainly

Table 2
Nd isotopic composition of granitic rocks of the BMC.

Sample	Nd (ppm)	Sm (ppm)	$^{147}Sm/^{144}Nd$	$^{143}Nd/^{144}Nd$		2σ	ε_{Nd}	T_{DM1} (Ma)	T_{DM2} (Ma)
G 151	94.64	23.59	0.1507	0.512839	±	7	5.0	523	752
G 155	28.62	4.833	0.1021	0.512809	±	6	5.5	344	467
G 231	73.41	25.87	0.2131	0.512906	±	6	4.9	–	–
G 234	77.21	15.97	0.1250	0.512819	±	6	5.2	412	569
G 237	83.26	20.04	0.1455	0.512856	±	14	5.4	452	657
G 244	62.07	13.77	0.1341	0.512810	±	8	4.8	474	651
LM 104	15.57	3.508	0.1362	0.512829	±	6	5.1	450	632
G 165	422.7	94.73	0.1355	0.512706	±	12	2.7	674	865
LM 99	410.1	85.75	0.1264	0.512729	±	8	3.4	568	733
LM 101	90.91	21.08	0.1402	0.512849	±	7	5.4	433	624

Samples: Peralkaline granite — G151, G155, G231, G234, G237, G244, LM 104; mineralized granite — G165, LM 99, LM101; $^{143}Nd/^{144}Nd$ are measured Nd isotopic ratios. The ε_{Nd} values were calculated assuming an age of 177 Ma. Concentrations of Nd and Sm were determined by isotope dilution. Nd model ages were calculated based upon De Paolo's (1988) depleted mantle model (T_{DM1}), and on a depleted mantle model (T_{DM2}) separated from the CHUR (chondrite-uniform reservoir) at 4.55 Ga, with linear evolution and a present-day epsilon value of +10.

Table 3
U–Th–Pb isotopic and concentration data for the granitic rocks and galena of the BMC.

Sample	U (ppm)	Th (ppm)	Pb (ppm)	$(206/204)_C$		2σ	$(207/204)_C$		2σ	$(208/204)_C$		2σ	$(206/204)_I$	$(207/204)_I$	$(208/204)_I$
G151	14.9	57.9	21.0	19.378	±	0.001	15.616	±	0.001	38.666	±	0.002	18.104	15.553	37.049
G155	7.6	18.2	14.0	19.597	±	0.001	15.607	±	0.001	38.744	±	0.003	18.614	15.558	37.979
G162	15.9	19.0	15.0	19.495	±	0.001	15.599	±	0.001	38.611	±	0.003	17.590	15.504	37.868
G231	22.1	25.6	14.0	20.150	±	0.002	15.619	±	0.001	38.856	±	0.004	17.279	15.477	37.770
G234	9.05	16.0	22.0	19.419	±	0.002	15.612	±	0.002	38.634	±	0.006	18.680	15.575	38.208
G237	14.3	17.1	29.0	19.555	±	0.001	15.609	±	0.001	38.684	±	0.003	18.667	15.565	38.377
G244	8.54	21.2	48.0	19.270	±	0.001	15.605	±	0.001	38.630	±	0.002	18.951	15.589	38.372
LM104	127	17.4	201	19.268	±	0.001	15.574	±	0.001	38.222	±	0.002	18.142	15.518	38.172
G165	34.2	56.4	89.0	19.546	±	0.001	15.626	±	0.001	38.959	±	0.004	18.852	15.592	38.585
LM99	16.6	59.0	40.0	19.361	±	0.001	15.601	±	0.001	38.760	±	0.002	18.615	15.564	37.894
LM101	52.1	64.3	18.0	23.012	±	0.001	15.765	±	0.001	39.685	±	0.002	17.481	15.491	37.456
galena				18.896	±	0.003	15.578	±	0.004	38.286	±	0.038			

Samples: Peralkaline granite — G151, G155, G162, G231, G234, G237, G244, LM 104; mineralized granite — G165, LM 99, LM101; $(206/204)_c$, $(207/204)_c$ and $(208/204)_c$ are measured $^{206}Pb/^{204}Pb$, $^{207}Pb/^{204}Pb$ and $^{208}Pb/^{204}Pb$ isotopic ratios respectively, corrected for mass fractionation. $(206/204)_i$, $(207/204)_i$ and $(208/204)_i$ are initial (time corrected) $^{206}Pb/^{204}Pb$, $^{207}Pb/^{204}Pb$ and $^{208}Pb/^{204}Pb$ ratios, respectively (assumed age 177 Ma). Galena — sample from the I & L Zone; $^{208}Pb/^{206}Pb$ (±2 σ) = 2.0265 ± 0.0004; $^{207}Pb/^{206}Pb$ = 0.82443 ± 0.0001; All isotopic ratios for galena corrected for mass fractionation to the values of Todt et al. (1996). For galena 2σ — reproducibility of NBS 981.

due to extensive fractional crystallization. Important in this context, however, are the high enrichment levels of Zr and REE both within pegmatites/felsic dikes and the intergranular (i.e., late crystallization volumes) parts of some granites, which may reflect the high levels of rare element enrichment attained during magmatic fractionation. However, mineralization is typically associated with altered parts of peralkaline intrusions and many rare metal-bearing minerals are post-magmatic (hydrothermal) phases and show replacement textures, which suggest that the metal enrichment is also related to hydrothermal activity.

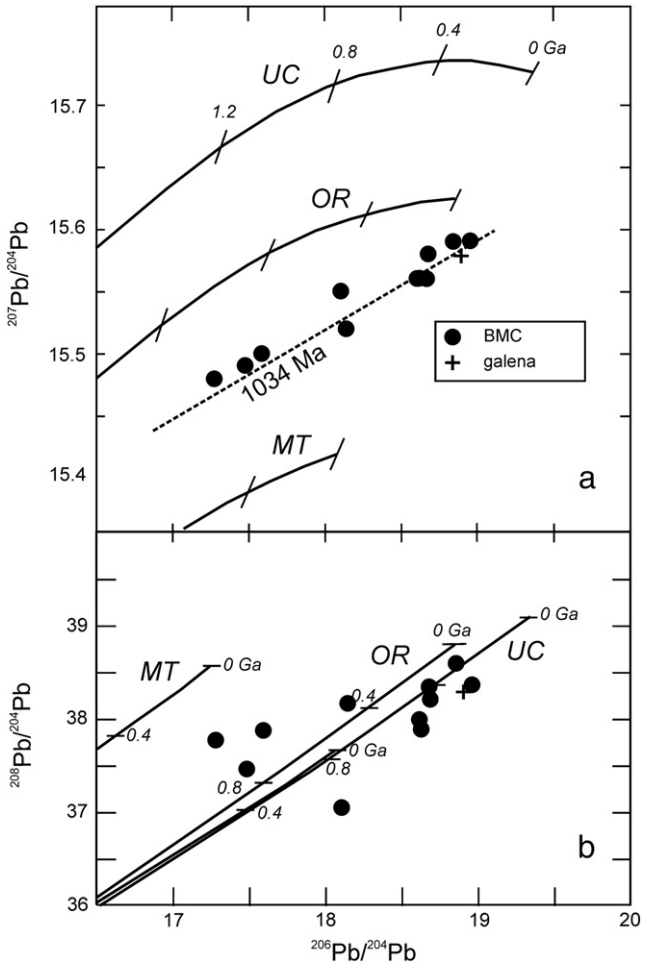

Fig. 11. Plots of lead isotopic data for Bokan Mountain granitic rock samples in $^{207}Pb/^{204}Pb$ versus $^{206}Pb/^{204}Pb$ (a) and $^{208}Pb/^{204}Pb$ versus $^{206}Pb/^{204}Pb$ (b) diagrams with lead evolution curves shown (from Doe and Zartman, 1979) for the mantle (MT), orogene (OR) and upper crust (UC). The reference isochron of 1034 Ma, which goes through the Bokan data in (a), is discussed in the text. Circle — peralkaline granites; cross — galena.

It has been documented elsewhere (e.g., Salvi and Williams-Jones, 2004) that volatiles play an important role in the evolution of highly evolved peralkaline rocks. The parent melts of the peralkaline felsic rocks are generated under dry conditions (Salvi and Williams-Jones, 2004), as attested in the case of BMC by the low modal abundance of amphibole and its late-stage appearance in the crystallization history of the complex. Consequently, when these magmas undergo extensive fractionation they become saturated with aqueous fluids only very late in their crystallization history. The presence of low-density fluid inclusions in the amphibole at Bokan may be evidence of such volatile enrichment in the late-stage magmatic evolution of the complex. At the advanced stage of fractionation, the aqueous fluids escape from the magma which, at this point in its evolution, is also highly enriched in incompatible elements (such as REE, HFSE, Th and U) and, in addition, may contain significant amounts of halogens, particularly fluorine. Thus, the hydrothermal fluids, which are enriched in all these elements, can play an important role in further concentrating the HFSE, REE, Th and U, as well as during autometasomatism (e.g., Salvi and Williams-Jones, 2004; Sheard et al., 2012).

Fluid saturation of the magma in the late stages of the magma evolution is suggested to have resulted in its rapid degassing and consequent release of highly fractionated, silica-saturated melts, subsequently followed by an escape of related highly evolved fluids. These fluids, which would have been localized to the most evolved parts of the highly fractionated magma, were enriched in F (as also indicated by a widespread occurrence of fluorite) and facilitated the complexing and mobility of REE and HFSE. The escaping fluids would have preferentially traveled along zones of structural weakness, likely corresponding to the present deformation zones, with the precipitation of the U, Th, REE and HFSE mineralization due to fluid-wall rock interaction and related changes in the fluid chemistry. These fluids also in part leached REE and HFSE from the earlier formed, primary magmatic phases, as has been discussed for other similar complexes (Salvi and Williams-Jones, 2004) and reprecipitated them in fractures and cavities, in addition to replacing earlier phases. The mineralization, therefore, records two distinct periods: the first relates to the late stage magmatic evolution of the Bokan complex, which is a product of fractional crystallization, whereas the second stage is associated with the release of orthomagmatic hydrothermal fluids at the terminal stage of magmatic evolution and

Table 4
Oxygen isotopic composition of quartz from BMC.

Sample	Host rock	Mineral	$\delta^{18}O_{V\text{-}SMOW}$ (‰)
LM66	Granite	Quartz	9.0
LM78	Granite	Quartz	8.9
Average			9.0
LM58	Vein/pegmatite	Quartz	11.3
LM61	Vein/pegmatite	Quartz	9.2
LM70	Vein/pegmatite	Quartz	8.9
LM71	Vein/pegmatite	Quartz	9.6
LM77	Vein/pegmatite	Quartz	9.3
Average			9.7

$\delta^{18}O_{V\text{-}SMOW}$ (‰) — the notation relative to V-SMOW (Vienna standard mean ocean water).

the ingress of this fluid into the already crystallized granitic rocks that comprise the BMC.

Mineralization of REE, as well as HFSE, U and Th, at the BMC is hosted by a variety of accessory and/or ore minerals. The primary magmatic accessory mineral paragenesis was extensively overprinted by younger hydrothermal event(s) that remobilized and enriched the REE, HFSE, U and Th and produced new mineral assemblages. Most of the REE- and HFSE-bearing minerals are post-magmatic phases which pseudomorphically replaced primary minerals. The proportions of LREE minerals (including bastnäsite and synchysite) and HREE minerals (including zircon, fergusonite and xenotime) are highly variable, particularly in the dikes due to the influence of late-stage orthomagmatic fluids which variably infiltrated and modified the minor and trace element contents of the samples. The significant variations of the REE patterns within the pluton (Fig. 7) and dikes (Fig. 10) with relatively uniform major element composition are consistent with an overprinting of granitic rocks by orthomagmatic hydrothermal fluids. Thus, the hydrothermal fluids redistributed and enriched the ITE, but did not significantly modify the major element composition. A distinct alteration aureole in granitoid country rocks around the contact with the pluton and the occurrence of fluorite veinlets rich in REE in the hornfelses attest to the important role of the fluids.

Although most of the BMC contains elevated concentrations of REE and HFSE as the results of both magmatic and (orthomagmatic) hydrothermal processes, the mineralization is preferentially associated with structurally-controlled alteration zones where post-magmatic-hydrothermal fluids circulated mainly along cracks and fractures.

Fluorite commonly occurs in the mineralized parts of the rocks and forms veinlets in the hornfelses around the contact with the complex. The presence of fluorite indicates an appreciable amount of fluorine in the aqueous fluids, suggesting that HFSE and REE might have been transported in hydrothermal fluids mainly as fluoride complexes. The interaction of such Ca-poor, F-rich fluids with Ca-bearing rocks or fluids would lead to the deposition of REE- and HFSE-bearing minerals, as well as fluorite (Salvi and Williams-Jones, 2004).

6.2.2. REE and Y deposits of peralkaline/alkaline felsic igneous rocks

Evolved peralkaline felsic igneous rocks host one of the most economically important resources of HREE and Y. These host rocks include nepheline syenites, peralkaline granites and trachytes and normally occur in continental intraplate settings. Typically, the REE and HFSE mineralization is closely related to the crystallization of magma, particularly to its late stages. The deposits and potential deposits can be grouped into three types. The first is associated with nepheline syenites of layered alkaline intrusions (e.g., Ilimaussaq, Greenland; Lovozero, Russia; Thor Lake/Nechalacho, NWT, Canada; Norra Kärr, Sweden; Pilanesberg, South Africa). The mineralization in these complexes occurs in layers with cumulate textures which indicate that the initial REE mineralization was of magmatic origin. The second type is related to peralkaline granitic rocks and the REE mineralization is hosted in pegmatites (including the NYF type of Cerny and Ercit, 2005) or in highly evolved peralkaline granitic bodies as disseminations (e.g., Strange Lake, Quebec-Labrador, Canada; Ghurayyah, Saudi Arabia; Khaldzan-Buregtey, Mongolia). Unlike the first type, this mineralization and its host rocks do not show any indication of crystal accumulation. The BMC belongs to this type although the mineralization is mainly hosted by structurally-controlled, late-magmatic to hydrothermal felsic dikes related to peralkaline granites. The last type is the REE and HFSE mineralization hosted by and disseminated in peralkaline felsic volcanic rocks (e.g., Dubbo Zirconia, Australia). The hosts of all these deposits are highly evolved alkaline/peralkaline felsic rocks. The deposits in nepheline syenites are more frequent whereas the deposits related to volcanic rocks are relatively rare. The only deposits of peralkaline felsic igneous rocks which are actively mined are those in Kola Peninsula (Lovozero) in Russia. Some others are in advanced stages of exploration.

All these exploitable or potentially exploitable peralkaline rock-hosted deposits have significantly higher content of HREE and Y, but lower LREE than those of carbonatites (Fig. 10). Also, when compared to carbonatite deposits, the REE patterns of the peralkaline deposits are distinctly shallower and display negative Eu anomalies (Fig. 10). The shapes of the REE patterns of the average ores from the peralkaline felsic rocks do not show systematic differences among the three types of deposits (Fig. 10) and most of them are overlapping, although within the individual deposits the REE patterns are highly variable (e.g. Fig. 10). However, there are subtle differences in the mineralogy of these deposits. For example, the deposits related to nepheline syenite contain eudialyte which is not typically present in the deposits associated with peralkaline granites. All these deposits display a late hydrothermal overprint and contain a variety of rare-metal minerals many of which typically show replacement textures (Verplanck et al., 2013). Furthermore, the relative proportions of primary and post-magmatic phases are variable within the individual deposits and the hydrothermal events appear to represent late stages of the evolution of the magmatic systems. Like at the BMC, the large variation of REE within the individual deposits associated with relatively small variations in the major element compositions combined with the textural evidence for hydrothermal overprinting in all these deposits suggest that the origin of the REE-HFSE deposits hosted by peralkaline/alkaline felsic rocks requires an emplacement of highly evolved magma with high contents of these elements where rocks and mineralization were subsequently modified by orthomagmatic hydrothermal fluids which remobilized and enriched the REE and partially replaced primary mineral assemblage by new minerals.

7. Conclusions

The proposed model for the evolution of the Jurassic Bokan complex invokes a parent mafic magma which was derived from a lithospheric mantle metasomatically enriched in HFSE, REE, Th and U, and probably halogens, thus suggesting that these source rocks were phlogopite and/or amphibole-bearing. These mantle melts (possibly alkali basalt) were modified by fractional crystallization during their ascent and subsequently in a high-level magma chamber where they underwent further differentiation resulting in the generation of extremely fractionated magma. Batches of this highly fractionated magma rose to form either a high-level stock or, alternatively (as Collot, 1981 suggested), the complex might represent the apex of the chamber. The extensive fractional crystallization recorded in the rocks likely occurred in the magma chamber (Cuney and Kyser, 2008).

The early-formed phases that dominate the evolved felsic magma, mainly alkali feldspar and quartz, do not contain any significant amounts of HFSE, REE, Th and U, thus their crystallization led to the further increase of the concentrations of these elements in the residual melt. At an advanced stage of fractional crystallization, the magma became fluid-saturated and over-pressured which resulted in the escape of both evolved melt and metal-rich fluid and the deposition of the U, Th, HFSE and REE mineralization which occurred preferentially in zones of structural weakness. The fluids were released from the late-stage, deep and hotter central part of the magma chamber and migrated towards the cooler, marginal part of the intrusion (Cuney and Kyser, 2008). These fluids not only produced mineralization, but also extensive microfracturing and pervasive alteration of the granites. The alteration included, but was not restricted to, the ubiquitous albitization of K-feldspar and partial dissolution of the quartz. This event was probably protracted with two or more stages of rare-metal enrichment. The occurrence of fluorite indicates that the fluids were also enriched in F and suggests that complexing of the REEs with fluorine played a role during their transportation (Salvi and Williams-Jones, 1990). Oxygen isotopes suggest that the mineralization and metasomatism occurred due to ingress of an orthomagmatic fluid and that this occurred in a closed system.

Melts and fluids also penetrated the country rocks along fractures and fault/shear zones for up to several km from the intrusive center. The occurrence of mineralized aplitic quartz-aegirine lenses within the structurally-controlled dikes suggests that the mineralization process already started during the magmatic stage. The mineralized bodies in these zones initially crystallized as peralkaline granitic pegmatites and aplites, but were extensively overprinted by hydrothermal fluids which also produced a significant metasomatic enrichment and remobilization of rare metals. It was during this fluid–rock interaction that most REE and HFSE minerals were formed. Thus, the deposits are the result of at least two periods of mineralization with both being associated with the late stages of magma evolution. The first period produced primary magmatic mineralization related to crystallization of highly fractionated peralkaline melts, whereas the second period involved the late magmatic to hydrothermal fluids which remobilized and enriched the original mineral assemblage during multiple events. These orthomagmatic fluids escaped during the last stages of the magma evolution. Other REE-HFSE deposits hosted by peralkaline felsic rocks (nepheline syenites, peralkaline granites and trachytes) also record two similar stages of mineralization.

Acknowledgments

We thank Nelson Eby, Erin Todd and two anonymous reviewers for constructive reviews of the manuscript. Support for this research was provided by the U.S. Geological Survey Mineral Resources External Research Grant G09AP00039, NSERC of Canada (Discovery grants to J.D. and D.K.) and Ucore Rare Metals Ltd. We would like to thank Randy Corney for technical assistance and Jim Barker for help with fieldwork and encouragement.

Appendix 1. Analytical techniques

1.1. Major and trace elements

Whole-rock major and trace elements in 48 samples (Appendix 2) were determined using lithium tetraborate fusion at the Activation Laboratories, Ancaster, Ontario, Canada. Major elements and some trace elements (Ba, Sr, Y and Zr) were determined by inductively coupled plasma-optical emission spectrometry, whereas other trace elements were analyzed using a Perkin Elmer Optima 3000 inductively coupled plasma mass spectrometer. Based on replicate analyses, the precision is generally between 2 and 10% for trace elements and 3–5% for major elements.

1.2. Nd isotopes

Ten whole-rock samples were selected for Nd isotopic analyses (Table 2). Samarium and Nd abundances and Nd isotopic ratios were determined by isotope dilution mass spectrometry in the laboratory of the Department of Earth Sciences at the Memorial University of Newfoundland (St. John's, Newfoundland, Canada). The precision of concentrations of Nd and Sm is ± 1%. The isotopic ratios were determined using a multicollector Finnigan MAT 262 V thermal ionization mass spectrometer operated in a static mode. Measured $^{143}Nd/^{144}Nd$ values were fractionation corrected to a natural $^{146}Nd/^{144}Nd$ value of 0.721903, normalized to the JNdi-1 standard ($^{143}Nd/^{144}Nd$ = 0.512115; Tanaka et al., 2000) with $^{143}Nd/^{144}Nd$ values accurate to <0.002% and the $^{147}Sm/^{144}Nd$ ratio accurate to <0.1%. Replicate analyses of JNdi-1 standard yielded $^{143}Nd/^{144}Nd = 0.512137 \pm 1$ (n = 112). The ε_{Nd} values were calculated assuming t = 177 Ma. Nd model ages (Table 2) were calculated based upon De Paolo's (1988) depleted mantle model (T_{DM1}), and on a depleted mantle model (T_{DM2}) separated from the CHUR (chondrite-uniform reservoir) at 4.55 Ga, with linear evolution and a present-day epsilon value of +10.

1.3. Pb isotopes

1.3.1. Whole rocks

Eleven whole-rock samples were analyzed for Pb isotopes with thermal ionization mass spectrometry (Table 3). For Pb isotopic analysis, about 0.2 g of rock powder was dissolved. Separation of Pb was done by the standard anionic HBr–HCl chromatography. Isotopic ratios were obtained using a multicollector Finnigan Mat 262 thermal ionization mass spectrometer in static and dynamic mode at the Department of Earth Sciences, Memorial University of Newfoundland (St. John's, Newfoundland, Canada). Pb isotopic ratios in Table 3 were corrected for mass fractionation (Table 3). A correction factor of 0.107% per amu was obtained by measuring the deviation from repeated (n = 12) analyses of the NBS 981 standard. In-run precisions on all isotopic ratios are given at a 95% confidence level.

1.3.2. Galena

Galena from a pegmatite dike of the I&L zone was separated from a crushed sample by handpicking mm-size grains using a binocular microscope. The galena was dissolved in 8 N HNO_3, dried and re-dissolved in HBr for Pb separation and isotopic analyses at the Department of Earth Sciences of Carleton University, Ottawa, Ontario, Canada. Pb purification was done using standard anion exchange techniques and Pb isotopes measured by thermal ionization mass spectrometry. Pb mass spectrometer data were corrected for fractionation using NBS SRM981. The average ratios measured for NBS SR981 are $^{206}Pb/^{204}Pb = 16.891 \pm 0.011$, $^{207}Pb/^{204}Pb = 15.430 \pm 0.014$, and $^{208}Pb/^{204}Pb = 36.505 \pm 0.048$ (2σ). The fractionation correction is +0.13%/amu (based on the values of Todt et al., 1996).

1.4. Oxygen isotopes

Seven samples of granitic material were analyzed for ^{18}O at the Queens's Facility for Isotope Research, Kingston (Ontario) using conventional methods (Table 4), as summarized in Kontak and Kyser (2009). Briefly, oxygen was extracted from quartz using the BrF_5 method of Clayton and Mayeda (1963) and isotopic measurements run on a dual inlet using a Finnigan MAT 252 isotope ration mass spectrometer. All values are reported using the δ notation (‰) relative to V-SMOW (Vienna standard mean ocean water) and replicate $\delta^{18}O$ analyses were reproducible to ± 0.3‰.

Appendix 2. Major (wt.%) and trace element (ppm) compositions of the BMC rocks

Sample	G-151	G-152	G-153	G-154	G-156	G-157	G-158	G-160	G-161	G-162	G-163	G-164	G-168	G-169	G-170	G-171	G-172	G-230	G-231	G-232	G-234	G-235	G-236	G-237
SiO_2	74.8	77.3	76.7	73.3	74.0	74.1	73.0	73.9	74.2	74.8	74.3	73.1	74.6	73.9	75.9	75.7	74.4	73.9	74.1	74.4	73.9	75.3	75.2	74.9
TiO_2	0.12	0.04	0.06	0.18	0.18	0.16	0.16	0.11	0.10	0.11	0.15	0.12	0.13	0.15	0.04	0.13	0.18	0.14	0.26	0.13	0.13	0.12	0.10	0.16
Al_2O_3	11.6	12.4	12.5	11.7	11.2	11.4	11.6	11.1	11.2	11.6	10.5	11.4	10.8	11.3	12.3	12.4	11.6	11.0	11.0	10.7	10.8	11.5	11.3	11.9
Fe_2O_3	3.91	0.81	1.62	4.34	4.05	3.94	4.00	3.69	3.53	3.82	4.36	4.58	3.99	4.20	1.15	1.38	4.51	4.15	4.35	4.83	4.35	4.16	4.43	3.75
MnO	0.08	0.01	0.02	0.08	0.05	0.06	0.06	0.08	0.03	0.05	0.05	0.04	0.05	0.01	0.02	0.04	0.04	0.04	0.03	0.09	0.03	0.02	0.05	0.04
MgO	0.02	0.01	0.08	0.01	0.01	0.02	0.02	0.01	0.01	0.03	0.02	0.01	0.02	0.01	0.03	0.47	0.03	0.01	0.01	0.02	0.02	0.02	0.02	0.02
CaO	0.11	0.18	0.15	0.12	0.02	0.30	0.08	0.04	0.24	0.03	0.03	0.11	0.02	0.17	0.19	0.53	0.06	0.02	0.34	0.06	0.07	0.11	0.04	0.29
Na_2O	5.51	4.28	4.42	4.52	4.35	4.70	4.85	4.81	5.25	4.94	4.37	4.72	4.81	3.95	4.24	4.12	5.34	5.06	4.17	6.16	5.66	5.93	5.25	4.99
K_2O	3.56	4.30	3.95	4.13	4.55	4.30	4.22	4.18	3.47	4.11	4.24	4.39	3.99	4.45	4.57	3.88	4.45	4.49	4.81	2.27	3.49	3.30	4.05	4.37
P_2O_5	0.03	0.01	0.04	0.01	0.01	0.01	0.02	0.01	0.01	0.01	0.01	0.01	0.01	0.01	0.01	0.02	0.02	0.01	0.01	0.01	0.01	0.01	0.01	0.01
LOI	0.34	0.48	0.22	0.57	0.49	0.80	0.53	0.36	0.29	0.31	0.38	0.48	0.33	0.40	0.24	0.57	0.33	0.28	0.72	0.29	0.33	0.30	0.19	0.39
Total	100.1	99.9	99.8	98.9	98.9	99.8	98.5	98.3	98.4	99.9	98.4	99.0	98.7	98.6	98.7	99.3	100.9	99.2	99.8	99.0	98.8	100.8	100.7	100.8
Pb	21	23	17	16	47	28	14	16	81	15	42	24	9	29	15	6	43	32	14	12	22	8	11	29
Zn	170	0	0	190	330	190	110	190	220	100	200	280	160	110	0	50	80	110	220	250	80	40	160	300
Sn	30.0	2.0	6.0	12.0	25.0	24.0	17.0	17.0	25.0	26.0	19.0	17.0	17.0	22.0	6.0	2.0	23.0	33.0	17.0	18.0	17.0	19.0	19.0	19.0
Rb	229	165	198	186	218	171	178	297	240	279	251	306	217	187	173	76	269	288	249	128	194	197	238	223
Cs	0.90	1.20	3.10	0.50	0.60	0.30	0.40	1.10	0.60	0.70	1.10	1.00	0.80	0.30	0.90	0.70	0.50	0.40	0.70	0.80	0.60	0.40	0.60	0.90
Ba	49	20	17	37	29	44	62	36	19	26	33	40	27	23	30	486	16	29	29	28	28	19	29	26
Sr	9	4	4	6	4	29	4	3	13	3	2	9	1	8	10	54	6	1	10	6	4	8	4	15
Ga	39	26	23	40	41	40	38	40	42	38	39	42	40	42	20	15	38	40	35	46	40	44	43	44
Ta	7.74	3.28	2.16	4.64	7.32	5.44	5.52	2.99	9.47	6.34	5.45	3.15	3.61	5.00	3.15	0.35	10.2	4.13	5.76	5.03	2.93	5.32	4.65	4.31
Nb	105	43.7	38.6	63.1	117	68.3	77.0	36.0	137	87.2	70.6	49.0	52.3	62.2	54.7	4.5	165	49.8	67.5	70.9	45.0	83.6	57.7	58.6
Hf	34.6	7.20	5.80	23.7	30	39.8	42.4	81.1	58	64.2	50.7	29.6	35.9	29.4	5.60	4.90	71.3	55.9	52.1	34.4	25.2	26.0	28.6	45.3
Zr	1520	119	120	1220	1310	1880	2030	3720	2750	3000	2470	1400	1670	1450	106	164	3640	2300	2250	1350	1050	1040	1150	1840
Y	182	20	11	92	52	211	129	253	264	150	39	76	36	121	36	29	77	65	349	107	61	88	34	111
Th	57.9	38.2	37.1	24.3	24.0	48.0	30.3	14.0	43	19.0	27.0	21.2	22.2	20.8	27.0	7.89	16.6	20.2	25.6	54.6	16.0	38.5	11.4	17.1
U	14.9	14.3	8.73	9.75	7.97	11.3	12.8	8.27	24	15.9	11.8	8.63	7.30	11.5	12.0	11.4	27.4	18.7	22.1	9.81	9.05	14.2	11.0	14.3
La	83.9	2.67	4.94	154	74.3	82.7	39.4	84.7	131	36.9	96.5	42.1	59.8	69.3	22.2	107	0.00	95.4	64.8	129	84.7	106	36.4	73.8
Ce	174	9.49	21.1	315	189	191	89.2	217	215	92.7	189	97.6	123	163	25.8	46.1	269	194	130	279	176	240	95.7	172
Pr	22.4	1.33	1.89	33.9	24.2	24.7	11.0	26.2	46	12.4	21.0	12.6	14.3	21.2	5.82	6.17	29.9	19.7	17.2	30.5	20.1	29.5	10.9	23.4
Nd	98.8	6.41	8.02	138	111	114	48.2	126	228	58.3	83.3	58.5	57.9	97.7	25.8	28.1	124	67.2	74.9	110	77.8	115	39.6	95.3
Sm	25.5	2.48	2.11	26.1	26.1	31.3	12.7	34.0	71	17.3	14.6	16.1	9.56	25.9	6.75	6.12	20.1	10.1	26.3	17.7	16.5	25.0	6.64	23.0
Eu	2.50	0.14	0.10	2.22	2.20	3.22	1.25	3.39	8.95	1.81	1.18	1.60	0.75	2.43	0.48	0.76	1.44	0.78	3.16	1.33	1.41	2.12	0.53	2.05
Gd	27.3	2.74	1.82	19.7	19.8	34.9	14.0	37.9	69	20.3	10.1	17.1	6.61	23.3	5.99	5.73	11.0	6.01	38.0	11.6	11.7	16.6	4.35	18.4
Tb	5.40	0.66	0.39	3.32	3.00	6.86	3.30	7.06	12	4.88	1.68	3.20	1.22	4.26	1.11	1.00	2.72	1.39	8.37	2.32	2.01	2.91	0.95	3.10
Dy	33.2	4.79	2.61	20.5	16.8	44.3	25.3	44.5	67	35.8	10.5	19.2	8.84	27.0	6.89	5.95	23.7	11.9	56.0	17.8	13.0	19.1	7.40	19.9
Ho	7.00	1.15	0.59	4.64	3.40	9.86	6.32	10.3	14	8.81	2.44	4.14	2.24	6.15	1.59	1.28	6.88	3.70	13.9	4.76	2.98	4.71	1.84	5.21
Er	19.7	3.84	1.88	15.9	10.4	29.5	20.0	31.8	40	29.4	8.85	12.7	8.54	19.4	5.33	3.81	28.9	17.7	50.1	18.3	8.95	17.5	6.67	19.7
Tm	3.25	0.78	0.36	3.37	1.93	4.88	3.59	5.64	7.02	5.58	2.00	2.39	1.91	3.62	1.01	0.63	7.18	5.08	10.6	3.86	1.94	3.71	1.38	4.17
Yb	20.7	5.42	2.44	26.2	14.2	28.8	23.6	37.4	45	37.9	16.9	17.0	15.1	24.1	7.04	4.10	59.8	45.4	79.1	29.6	14.0	27.9	11.0	30.1
Lu	2.82	0.81	0.35	3.99	2.20	3.78	3.43	5.52	5.91	5.36	2.88	2.57	2.50	3.44	1.08	0.61	9.22	7.16	11.8	4.45	2.19	4.11	1.78	4.33

Samples: G — Bokan Mountain Complex; LM — Dotson and I&L zones; locations of samples in Dostal et al. (2011).

(*continued on next page*)

Appendix 2 *(continued)*

Sample	G-238	G-239	G-240	G-241	G-242	G-243	G-245	G-246	LM-14	LM-15	LM-16	LM-17	LM-19	LM-93	LM-95	LM-96	LM-97	LM-99	LM-100	LM-102	LM-103	LM-105	LM-106	LM-145
SiO_2	76.9	76.4	74.2	77.6	72.1	73.9	73.0	72.7	74.1	73.6	74.5	73.7	73.9	72.5	73.8	73.3	72.5	73.6	73.5	75.2	74.6	73.2	76.8	73.3
TiO_2	0.12	0.11	0.17	0.12	0.14	0.16	0.20	0.17	0.13	0.14	0.15	0.15	0.16	0.15	0.14	0.19	0.18	0.16	0.15	0.11	0.14	0.11	0.09	0.15
Al_2O_3	10.3	10.8	11.9	9.2	11.1	12.0	12.3	12.3	11.2	10.7	10.7	11.0	11.5	11.3	11.1	9.5	11.3	10.9	10.8	11.6	10.5	10.9	11.0	10.6
Fe_2O_3	4.19	4.63	4.18	5.99	5.32	4.52	3.43	3.39	3.72	4.13	4.22	4.12	4.46	5.27	4.52	6.89	3.92	4.08	4.36	3.42	4.56	4.57	3.33	4.82
MnO	0.03	0.01	0.09	0.13	0.11	0.06	0.09	0.07	0.14	0.07	0.04	0.08	0.14	0.04	0.02	0.09	0.02	0.05	0.08	0.03	0.05	0.07	0.04	0.03
MgO	0.02	0.01	0.02	0.01	0.02	0.02	0.02	0.02	0.02	0.01	0.01	0.01	0.03	0.02	0.01	0.01	0.01	0.01	0.01	0.02	0.01	0.02	0.02	0.02
CaO	0.04	0.02	0.17	0.05	0.06	0.03	0.06	0.27	0.18	0.30	0.28	0.40	0.58	0.38	0.51	0.20	1.45	0.36	0.37	0.27	0.88	0.43	0.29	0.30
Na_2O	4.15	4.04	4.77	6.66	5.16	4.76	5.62	5.48	3.52	4.45	5.25	4.49	4.53	4.15	3.99	5.69	3.94	5.09	5.10	4.90	3.84	4.87	3.68	4.59
K_2O	3.83	3.96	4.38	0.51	4.41	5.15	3.99	3.90	5.44	4.58	3.75	4.75	3.38	4.50	4.26	2.99	4.22	4.02	4.02	3.73	3.75	3.73	4.08	4.28
P_2O_5	0.02	0.01	0.02	0.01	0.01	0.01	0.01	0.10	0.04	0.01	0.01	0.01	0.01	0.01	0.01	0.01	0.01	0.01	0.02	0.01	0.01	0.01	0.02	0.01
LOI	0.25	0.44	0.55	0.25	0.32	0.12	0.33	0.45	0.51	0.50	0.47	0.58	0.78	0.50	0.45	0.59	0.95	0.53	0.51	0.40	0.92	0.57	0.93	0.51
Total	99.9	100.5	100.4	100.5	98.7	100.8	99.0	98.9	99.1	98.4	99.4	99.2	99.4	98.9	98.8	99.5	98.4	98.8	99.0	99.7	99.2	98.6	100.2	98.7
Pb	9	11	88	18	32	7	37	46	5	52	6	8	9	10	15	18	13	40	7	8	8	16	25	7
Zn	130	60	220	390	330	160	200	180	50	300	210	260	290	140	250	220	90	340	290	140	240	190	290	300
Sn	13.0	20.0	23.0	10.0	21.0	18.0	33.0	14.0	16.0	22.0	28.0	20.0	30.0	14.0	21.0	30.0	29.0	29.0	25.0	11.0	18.0	16.0	9.0	29.0
Rb	194	191	243	18	307	324	224	198	222	236	180	234	141	206	182	162	212	224	223	246	197	196	219	225
Cs	0.70	0.90	0.70	1.00	1.80	1.30	1.10	1.70	0.40	0.40	0.30	0.40	0.20	0.40	0.40	0.40	0.40	0.50	0.80	0.60	0.30	0.90	0.70	0.40
Ba	34	25	114	6	29	28	55	82	43	26	28	24	32	45	43	23	20	31	27	44	15	20	25	35
Sr	3	1	13	1	3	1	5	10	10	9	10	20	37	27	24	9	33	19	1616	15	18	28	14	8
Ga	41	42	45	45	45	39	40	40	36	37	40	39	43	37	41	38	36	43	39	39	39	40	43	41
Ta	2.82	3.68	4.22	2.36	5.03	2.38	6.32	6.02	5.33	10.9	11.1	10.7	15.5	7.18	2.89	4.09	4.03	9.34	7.25	2.48				8.58
Nb	39.1	51.9	58.5	36.3	64.8	37.0	83.0	74.5	90.7	180	166	180	237	96.9	53.5	69.8	60.6	134	113	39.0	62.2	58.3	49.5	119
Hf	23.8	27.9	39.8	14.2	72.9	17.8	45.9	32.9	29.0	29.4	47.9	42.9	21.9	7.80	11.7	11.5	50.1	58	61	11.8	57.6	15.5	5.80	38
Zr	931	1060	1530	607	2720	707	1810	1080	1420	1270	2160	1990	1240	249	369	376	2450	2520	2990	416	2920	649	254	1820
Y	37	46	131	30	341	43	238	286	239	237	244	263	405	269	429	98	151	149	194	230	144	110	125	294
Th	21.4	27.7	29.5	13.5	23.4	16.9	39.5	49.6	186	44.8	17.6	22.4	47.1	29.7	17.2	12.8	28.6	59	26	10.6	22.8	22.2	25.2	49
U	6.73	8.72	15.6	5.99	17.4	5.32	20.0	27.2	17.9	20.9	20.0	20.8	33.9	11.9	5.45	8.81	17.0	17	22	7.44	26.0	7.81	7.12	23
La	56.6	48.7	205	33.3	110	21.4	113	113	63.2	79.6	101	95.0	231	68.7	95.9	57.4	95.0	345	138	45.4	96.4	106	267	178
Ce	137	121	450	109	200	55.8	322	314	158	187	241	224	616	164	221	139	202	846	366	112	213	227	577	431
Pr	17.5	14.9	52.3	7.52	34.9	4.76	31.0	37.9	21.0	23.2	30.3	27.9	69.1	21.5	28.5	18.0	24.4	93	47	15.1	26.3	27.4	56.7	54
Nd	67.7	58.5	208	23.9	144	17.1	124	154	96.4	102	137	124	306	99.3	130	81.8	108	408	214	73.1	117	119	228	246
Sm	13.8	11.6	40.5	3.85	42.7	3.48	31.7	44.3	25.2	29.3	37.7	34.8	76.2	29.4	38.6	21.0	26.2	90	61	20.1	27.8	25.2	41.1	63
Eu	1.11	0.94	3.41	0.34	4.46	0.34	3.12	4.48	2.61	3.14	3.82	3.49	7.21	3.18	4.27	1.98	2.42	7.66	5.68	2.02	2.54	2.33	3.42	5.74
Gd	8.68	8.20	31.00	2.78	47.0	3.30	32.2	43.3	30.0	34.9	40.3	36.2	73.8	35.7	50.7	19.9	24.5	65	58	23.4	24.8	23.2	31.7	56
Tb	1.39	1.58	5.06	0.68	10.3	0.87	6.49	9.29	6.81	7.75	8.01	7.84	13.3	7.53	10.6	3.67	4.34	8.55	8.68	5.56	4.57	4.12	4.91	9.82
Dy	8.52	11.0	30.4	5.70	66.6	6.97	42.1	58.4	48.4	51.8	49.5	52.5	77.9	48.5	67.0	22.1	29.8	42	48	40.0	30.6	24.4	27.7	61
Ho	1.94	2.64	8.25	1.63	14.9	1.83	9.39	12.2	12.0	11.2	10.3	11.9	15.8	10.4	14.1	4.57	7.49	7.74	9.49	9.51	7.20	5.04	5.45	14
Er	7.00	9.38	19.1	6.94	45.5	6.44	28.1	35.6	40.2	30.6	27.3	33.0	43.2	28.1	36.4	13.0	25.1	23	27	28.9	23.1	14.1	14.9	42
Tm	1.59	1.94	3.40	1.77	7.88	1.31	4.55	6.12	7.39	4.39	4.01	4.86	6.91	4.01	5.09	2.28	4.71	4.02	4.39	5.10	4.65	2.33	2.25	7.43
Yb	13.3	15.5	24.1	15.0	51.8	10.0	28.3	40.2	47.0	25.7	23.6	27.5	42.2	23.2	28.8	16.6	32.0	28	29	33.6	36.1	15.2	13.3	49
Lu	2.20	2.41	3.43	2.42	7.39	1.58	3.74	4.92	6.63	3.62	3.28	3.72	5.61	3.18	4.10	2.76	4.49	3.92	4.27	4.77	5.56	2.19	1.82	6.79

References

Abdel-Rahman, A.M., 2006. Petrogenesis of anorogenic peralkaline granitic complexes from eastern Egypt. Mineralogical Magazine 70, 27–50.

Ayuso, R.A., Karl, S.M., Slack, J.F., Haeussler, P.J., Bittenbender, P.E., Wandless, G.A., Colvin, A.S., 2007. Oceanic Pb-isotopic sources of Proterozoic and Paleozoicvolcanogenic massive sulfide deposits on Prince of Wales Island and vicinity. U.S. Geological Survey Professional Paper 1732-E. Alaska Science Centre, Southeastern Alaska.

Barker, J.C., Van Gosen, B.S., 2012. Alaska's rare earth deposit and resource potential. Mining Engineering 64, 20–32.

Bonin, B., 2007. A-type granites and related rocks: evolution of a concept, problems and prospects. Lithos 97, 1–29.

Bottinga, Y., Javoy, M., 1973. Comments on oxygen isotope geothermometry. Earth and Planetary Science Letters 20, 250–265.

Bowden, P., Turner, D.C., 1985. Peralkaline and associated ring-complexes in the Nigeria-Niger Province, West Africa. In: Sørensen, H. (Ed.), The Alkaline Rocks. Wiley, London, pp. 330–351.

Castor, S.B., 2008. The Mountain Pass rare-earth carbonatite and associated ultrapotassic rocks, California. Canadian Mineralogist 46, 779–806.

Cathles, L.M., 1993. Oxygen isotope alteration in the Noranda mining district, Abitibi Greenstone Belt, Quebec. Economic Geology 88, 1483–1511.

Cerny, P., Meintzer, R.E., Anderson, A.J., 1985. Extreme fractionation in rare element granitic pegmatites: selected examples of data and mechanisms. Canadian Mineralogist 23, 381–421.

Cerny, P., Ercit, T.S., 2005. Classification of granitic pegmatites revisited. Canadian Mineralogist 43, 2005–2026.

Cerny, P., Blevin, P.L., Cuney, M., London, D., 2005. Granite-related ore deposits. Economic Geology 100, 337–370.

Chakhmouradian, A.R., Zaitsev, A.N., 2012. Rare earth mineralization in igneous rocks: sources and processes. Elements 8, 347–353.

Civetta, L., D'Antonio, M., Orsi, G., Tilton, G.R., 1998. The geochemistry of volcanic rocks from Pantelleria Island, Sicili Channel: petrogenesis and characteristics of the mantle source region. Journal of Petrology 39, 1453–1491.

Clayton, R.N., Mayeda, T.K., 1963. The use of bromine pentafluoride in the extraction of oxygen from oxides and silicates for isotopic analysis. Geochimica et Cosmochimica Acta 27, 43–52.

Collins, W.J., Beams, S.D., White, A.J.R., Chappell, B.W., 1982. Nature and origin of A-type granites with particular reference to Southeastern Australia. Contributions to Mineralogy and Petrology 80, 189–200.

Collot, B., 1981. Le granite albitique hyperalcalin de Bokan Mountain (S.E. Alaska) et ses mineralisations U – Th. Sa place dans la cordilliere canadienne. Doct. 3 degree cycle thesis Montpellier II University, Montpellier, France, (238 pp.).

Cox, K.G., Bell, J.D., Pankhrust, R.J., 1979. The Interpretation of Igneous Rocks. George Allen & Unwin, London, (450 pp.).

Cuney, M., Kyser, T.K., 2008. Deposits related to magmatic differentiation. In: Cuney, M., Kyser, K. (Eds.), Recent and Not-so Recent Developments in Uranium Deposits and Its Implications for Exploration. Mineralogical Association of Canada Short Course, vol. 39, pp. 55–77.

DePaolo, D.J., 1988. Neodymium Isotope Geochemistry: An Introduction. Springer Verlag, New York, (187 pp.).

Doe, B.R., Zartman, R.E., 1979. Plumbotectonics, the Phanerozoic, In: Barnes, H.L. (Ed.), Geochemistry of Hydrothermal Ore Deposits, 2nd ed. Wiley-Interscience, New York, pp. 22–70.

Dostal, J., Chatterjee, A.K., 1995. Origin of topaz-bearing and related peraluminous granites of late Devonian Davis Lake pluton, Nova Scotia, Canada. Chemical Geology 123, 67–88.

Dostal, J., Chatterjee, A.K., 2000. Contrasting behaviour of Nb/Ta and Zr/Hf ratios in a peraluminous granitic pluton (Nova Scotia, Canada). Chemical Geology 163, 207–218.

Dostal, J., Kontak, D.J., Hanley, J., Owen, V., 2011. Geological investigation of rare earth element and uranium deposits of the Bokan Mountain complex, Prince of Wales Island, southeastern Alaska. U.S. Geological Survey Mineral Resources External Research Program — Report GO9PA00039 (122 pp.).

Dostal, J., Karl, S.M., Keppie, J.D., Kontak, D.J., Shellnutt, J.G., 2013. Bokan Mountain peralkaline granitic complex, Alexander terrane (southeastern Alaska): evidence for Early Jurassic rifting prior to accretion with North America. Canadian Journal of Earth Sciences 50, 678–691.

Eby, G.N., 1990. The A-type granitoids: a review of their occurrence and chemical characteristics and speculations on their petrogenesis. Lithos 26, 115–134.

Eby, G.N., 1992. Chemical subdivision of the A-type granitoids: petrogenetic and tectonic implications. Geology 20, 641–644.

Frost, B.R., Barnes, C.G., Collins, W.J., Arculus, R.J., Ellis, D.J., Frost, C.D., 2001. A geochemical classification for granitic rocks. Journal of Petrology 42, 2033–2048.

Frost, C.D., Frost, B.R., 2011. On ferroan (A-type) granitoids: their compositional variability and modes of origin. Journal of Petrology 52, 39–53.

Gehrels, G.E., 1992. Geologic map of the southern Prince of Wales Island, southeastern Alaska. U. S. Geological Survey, Miscellaneous Investigations, Map1-2169, scale 1:63,000.

Goodenough, K.M., Upton, B.G.J., Ellam, R.M., 2000. Geochemical evolution of the Ivigtut Granite, South Greenland: a fluorine-rich "A-type" intrusion. Lithos 51, 205–221.

Halama, R., Marks, M., Brugmann, G., Siebel, W., Wenzel, T., Markl, G., 2004. Crustal contamination of mafic magmas: evidence from a petrological, geochemical and Sr–Nd–Os–O isotopic study of the Proterozoic Isortoq dike swarm, South Greenland. Lithos 74, 199–232.

Hatch, G.P., 2014. TMR Advanced Rare-Earth Projects Index. Technology Metal Research, March 2014. Available on line at http://www.techmetalsresearch.com/metrics-indices/tmr-advanced-rare-earth-projects-index/.

Hornig-Kjarsgaard, I., 1998. Rare earth elements in sövitic carbonatites and their mineral phases. Journal of Petrology 39, 2105–2121.

Keppler, H., 1993. Influence of fluorine on the enrichment of high field strength trace elements in granitic rocks. Contributions to Mineralogy and Petrology 114, 479–488.

Kontak, D.J., Kyser, T.K., 2009. Nature and origin of an LCT-suite pegmatite with late-stage sodium enrichment, Brazil Lake, Yarmouth Country, Nova Scotia. II. Implications of stable isotopes ($\delta^{18}O$, δD) for magma source, internal crystallization and nature of sodium metasomatism. Canadian Mineralogist 47, 745–764.

Kovalenko, V.I., Tsaryava, G.M., Goreglyad, A.V., Yarmolyuk, V.V., Troitsky, V.A., Hervig, R.L., Farmer, G.L., 1995. The peralkaline granite-related Khaldzan-Buregtey rare metal (Zr, Nb, REE) deposit, western Mongolia. Economic Geology 90, 530–547.

Kynicky, J., Chakhmouradian, A.R., Xu, C., Krmicek, L., Galiova, M., 2011. Distribution and evolution of zirconium mineralization in peralkaline granites and associated pegmatites of the Khan Bogd complex, southern Mongolia. Canadian Mineralogist 49, 947–965.

Kyser, T.K., 1986. Stable isotope variations in the mantle. In: Valley, J.W., Taylor Jr., H.P., O'Neil, J.R. (Eds.), Stable Isotopes in High Temperature Geological Processes. Reviews in Mineralogy, 16. Mineralogical Society of America, pp. 141–164.

Lentz, D.R., 1996. U, Mo and REE mineralization in late tectonic granitic pegmatites, Southwestern Grenville province, Canada. Ore Geology Review 11, 197–227.

Linnen, R.L., 1998. The solubility of Nb–Ta–Zr–Hf–W in granitic melts with Li and Li–F: constraints for mineralization in rare-metal granites and pegmatites. Economic Geology 93, 1013–1025.

Linnen, R.L., Cuney, M., 2004. Granite-related rare-element deposits and experimental constraints on Ta–Nb–W–Sn–Zr–Hf mineralization. In: Linnen, R.L., Samson, I.M. (Eds.), Rare-element Geochemistry and Mineral Deposits. Geological Association of Canada Short Course Notes, vol. 17, pp. 45–68.

Linnen, R.L., Keppler, H., 1997. Columbite solubility in granitic melts: consequences for the enrichment and fractionation of Nb and Ta in the Earth's crust. Contributions to Mineralogy and Petrology 128, 213–227.

Linnen, R.L., Keppler, H., 2002. Melt composition control on Zr/Hf fractionation in magmatic processes. Geochimica et Cosmochimica Acta 66, 3293–3301.

Long, K.R., Van Gosen, B.S., Foley, N.K., Cordier, D., 2010. The principal rare earth element deposits of the United States—a summary of domestic deposits and a global perspective. U.S. Geological Survey, Scientific Investigations Report 2010-5220 (96 pp.).

MacKevett Jr., E.M., 1963. Geology and ore deposits of the Bokan Mountain uranium–thorium area, southeastern Alaska. U. S. Geological Survey Bulletin 1154 (125 pp.).

Markl, G., Marks, M., Schwinn, G., Sommer, H., 2001. Phase equilibrium constraints on intensive crystallization parameters of the Ilimaussaq Complex, South Greenland. Journal of Petrology 42, 2231–2258.

Marks, M., Markl, G., 2001. Fractionation and assimilation processes in the alkaline augite syenite unit of the Ilímaussaq intrusion, South Greenland, as deduced from phase equilibria. Journal of Petrology 42, 1947–1969.

Marks, M., Vennemann, T., Siebel, W., Markl, G., 2003. Quantification of magmatic and hydrothermal processes in a peralkaline syenite-alkali granite complex based upon textures, phase equilibria, and stable and radiogenic isotopes. Journal of Petrology 44, 1247–1280.

Martin, R.F., De Vito, C., 2005. The patterns of enrichment in felsic pegmatites ultimately depend on tectonic setting. Canadian Mineralogist 43, 2027–2048.

Matsuhisa, Y., Goldsmith, J.R., Clayton, R.N., 1979. Oxygen isotopic fractionation in the system quartz–albite–anothite–water. Geochimica et Cosmochimica Acta 43, 1131–1140.

Mungall, J.E., Martin, R.F., 1996. Extreme differentiation of peralkaline rhyolite, Terceira, Azores: a modern analogue of Strange Lake, Labrador? Canadian Mineralogist 34, 769–777.

Philpotts, J.A., Taylor, C.D., Tatsumoto, M., Belkin, H.E., 1998. Petrogenesis of late-stage granites and Y–REE–Zr–Nb-enriched vein dikes of the Bokan Mountain stock, Prince of Wales Island, southeastern Alaska. U.S. Geological Survey, OF Report 98-459 (71 pp.).

Pilet, S., Baker, M.B., Stolper, E.M., 2008. Metasomatized lithosphere and the origin of alkaline lavas. Science 320, 916–919.

Pillet, D., Chenevoy, M., Belanger, M., 1992. Petrologie du granite peralcalin du Lac Brisson, Labrador central, Nouveau Quebec: 1. Mode de mise en palce et evolution chimique. Canadian Journal of Earth Sciences 29, 353–372.

Platt, R.G., 1996. Nepheline syenite complexes—an overview. In: Mitchell, R.H. (Ed.), Undersaturated Alkaline Rocks: Mineralogy, Petrogenesis and Economic Potential. Mineralogical Association of Canada Short Course Notes, vol. 24, pp. 63–99.

Richardson, D.G., Birkett, T.C., 1996. Peralkaline rock-associated rare metals. The Geology of North America, Geological Society of America, vol. P-1, pp. 523–540.

Robinson, R.J., Power, M.A., Barker, J.C., 2011. Technical report on the exploration program and mineral resource estimate for the Bokan Mountain Property, Prince of Wales Island, Alaska: NI 43-101 Report (190 pp.; accessed at http://ucore.com/projects/bokan-mountain-alaska/43-101).

Ronga, F., Lustrino, M., Marzoli, A., Melluso, L., 2010. Petrogenesis of a basalt-comendite-pantellerite rock suite: the Boseti Volcanic Complex (Main Ethiopian Rift). Mineralogy and Petrology 98, 227–243.

Salvi, S., Williams-Jones, A.E., 1990. The role of hydrothermal processes in the granite-hosted Zr, Y, REE deposit at Strange Lake, Quebec/Labrador: evidence from fluid inclusions. Geochimica et Cosmochimica Acta 54, 2403–2418.

Salvi, S., Williams-Jones, A.E., 1996. The role of hydrothermal processes in concentrating HFSE in the Strange Lake peralkaline complex, northeastern Canada. Geochimica et Cosmochimica Acta 60, 1917–1932.

Salvi, S., Williams-Jones, A.E., 2004. Alkaline granite–syenite deposits. In: Linnen, R.L., Samson, I.M. (Eds.), Rare-element Geochemistry and Mineral Deposits. Geological Association of Canada Short Course Notes, vol. 17, pp. 315–341.

Samson, S.D., McClelland, W.C., Patchett, P.J., Gehrels, G.E., Anderson, R.G., 1989. Evidence from neodymium isotopes for mantle contributions to Phanerozoic crustal genesis in the Canadian Cordillera. Nature 337, 705–709.

Schmitt, A.K., Trumbull, R.B., Dulski, P., Emmermann, R., 2002. Zr–Nb–REE mineralization in peralkaline granites from the Amis complex, Brandberg (Namibia): evidence for magmatic pre-enrichment from melt inclusions. Economic Geology 97, 399–413.
Sheard, E.R., Williams-Jones, A.E., Heoligmann, M., Pederson, C., Trueman, D.L., 2012. Controls on the concentration of zirconium, niobium, and the rare earth elements in the Thor Lake rare metal deposit, Northwest Territories, Canada. Economic Geology 107, 81–104.
Sheppard, S.M.F., 1986. Characterization and isotopic variations in natural waters. In: Valley, J.W., Taylor Jr., H.P., O'Neil, J.R. (Eds.), Stable Isotopes in High Temperature Geological Processes. Reviews in Mineralogy, 16, pp. 165–183.
Slack, J.F., Shanks, W.C., Karl, S.M., Gemery, P.A., Bittenbender, P.E., Ridley, W.I., 2007. Geochemical and sulfur-isotopic signatures of volcanogenic massive sulfide deposits on Prince of Wales Island and vicinity, southeastern. U. S. Geological Survey Professional Paper 1732-C. Alaska Science Centre, Alaska.
Staatz, M.H., 1978. I&L uranium and thorium vein system, Bokan Mountain, southern Alaska. Economic Geology 73, 512–523.
Stoeser, D.B., 1986. Distribution and tectonic setting of plutonic rocks of the Arabian Shield. Journal of African Earth Sciences 4, 21–46.
Sun, S.S., McDonough, W.F., 1989. Chemical and isotopic systematics of oceanic basalts: implications for mantle composition and processes. In: Saunders, A.D., Norry, M.J. (Eds.), Magmatism in the Ocean Basins. Geological Society London Special Publication, vol. 42, pp. 313–345.
Tanaka, T., et al., 2000. JNdi-1: a Neodymium isotopic reference in consistency with La Jolla Neodymium. Chemical Geology 168, 279–281.
Taylor Jr., H.P., 1986. Igneous rocks: II. Isotopic case studies of Circumpacific magmatism. In: Valley, J.W., Taylor Jr., H.P., O'Neil, J.R. (Eds.), Stable Isotopes in High Temperature Geological Processes. Reviews in Mineralogy, 16, pp. 273–317.
Taylor Jr., H.P., Sheppard, S.M.F., 1986. Igneous rocks: I. Processes of isotopic fractionation and isotope systematics. In: Valley, J.W., Taylor Jr., H.P., O'Neil, J.R. (Eds.), Stable Isotopes in High Temperature Geological Processes. Reviews in Mineralogy, 16, pp. 227–271.
Taylor, S.R., McLennan, S.M., 1985. The Continental Crust: Its Composition and Evolution. Blackwell, Oxford, (312 pp.).
Thompson, T.B., 1988. Geology and uranium–thorium mineral deposits of the Bokan Mountain granite complex, southeastern Alaska. Ore Geology Reviews 3, 193–210.
Thompson, T.B., Pierson, J.R., Lyttle, T., 1982. Petrology and petrogenesis of the Bokan granite complex, southeastern Alaska. Geological Society of America Bulletin 93, 898–908.
Todt, W., Cliff, R.A., Hanser, A., Hofmann, A.W., 1996. Evaluation of a 202Pb–205Pb double spike for high precision lead isotope analysis. In: Basu, A., Hart, S.R. (Eds.), Earth Processes: Reading the Isotopic Code. American Geophysical Union, Geophysical Monograph, vol. 95, pp. 429–437.
Upton, B.G.J., Emeleus, C.H., Heaman, L.M., Goodenough, K.M., Finch, A.A., 2003. Magmatism of the mid-Proterozoic Garder Province, South Greenland: chronology, petrogenesis and geological setting. Lithos 68, 43–65.
Verplanck, P.L., Van Gosen, B.S., Seal, R.R., McCafferty, A.E., 2013. A deposit model for carbonatite and alkaline intrusion-related rare earth element deposits. U.S. Geological Survey, Scientific Investigations Report 2010-5070-J.
Walters, A.S., Goodenough, K.M., Hughes, H.S.R., Roberts, N.M.W., Gunn, A.G., Rushton, J., Lacinska, A., 2013. Enrichment of rare earth elements during magmatic and post-magmatic processes: a case study from the Loch Loyal syenite complex, northern Scotland. Contributions to Mineralogy and Petrology 166, 1177–1202.
Warner, J.D., Barker, J.C., 1989. Columbium and rare earth-bearing deposits at Bokan Mountain, Southeast Alaska. Open-File Report 33-89. U. S. Bureau of Mines (196 pp.).
Whalen, J.B., Currie, K.L., Chappell, B.W., 1987. A-type granites: geochemical characteristics, discrimination and petrogenesis. Contributions to Mineralogy and Petrology 95, 407–419.
Winter, J.D., 2001. An Introduction to Igneous and Metamorphic Petrology. Prentice Hall, New Jersey, (697 pp.).